Friction **9**(3): 429–470 (2021)
https://doi.org/10.1007/s40544-020-0446-4
ISSN 2223-7690
CN 10-1237/TH

REVIEW ARTICLE

A review on tribology of polymer composite coatings

Yilong REN[1], Lin ZHANG[1], Guoxin XIE[1,*], Zhanbo LI[1], Hao CHEN[1], Hanjun GONG[1], Wenhu XU[2], Dan GUO[1], Jianbin LUO[1,*]

[1]*State Key Laboratory of Tribology, Department of Mechanical Engineering, Tsinghua University, Beijing 100084, China*
[2]*School of Mechatronics Engineering, Key Laboratory of Tribology, Nanchang University, Nanchang, Jiangxi 33003, China*

Received: 25 April 2020 / Revised: 10 July 2020 / Accepted: 18 August 2020

Abstract: Self-lubricating polymer composite coatings, with tailorable tribological and mechanical properties, have been widely employed on mechanical parts to reduce friction and wear, which saves energy and improves the overall performance for applications such as aerospace satellite parts, shafts, gears, and bushings. The addition of functional fillers can overcome the limitations of single-polymer coatings and extend the service life of the coatings by providing a combination of low friction, high wear resistance, high load bearing, high temperature resistance, and high adhesion. This paper compares the heat resistance, and the tribological and mechanical properties of common polymer matrices, as well as the categories of functional fillers that improve the coating performance. Applicable scopes, process parameters, advantages, and limitations of the preparation methods of polymer coatings are discussed in detail. The tribological properties of the composite coatings with different matrices and fillers are compared, and the lubrication mechanisms are analyzed. Fillers reduce friction by promoting the formation of transfer films or liquid shear films. Improvement of the mechanical properties of the composite coatings with fillers of different morphologies is described in terms of strengthening and toughening mechanisms, including a stress transfer mechanism, shear yielding, crack bridging, and interfacial debonding. The test and enhancement methods for the adhesion properties between the coating and substrate are discussed. The coating adhesion can be enhanced through mechanical treatment, chemical treatment, and energy treatment of the substrate. Finally, we propose the design strategies for high-performance polymer composite coating systems adapted to specific operating conditions, and the limitations of current polymer composite coating research are identified.

Keywords: polymer coatings; tribological properties; mechanical properties; adhesion properties; coating design

1 Introduction

As the demand for energy-efficient machines and environmental cleanliness continues to grow, a number of techniques have been developed to reduce friction and wear, save energy, and minimize waste. Because the use of liquid lubricants is limited by environmental considerations and is ill-suited for severe application conditions (such as high vacuum, high load, and extremely low or high temperature), solid lubricants in the form of coatings have been increasingly used to achieve low friction and low wear of moving mechanical parts. Significant progress has been made in the design, development, and use of solid lubricating coatings. Polymer coatings play a significant role in adjusting the interfacial properties of solid

* Corresponding authors: Guoxin XIE, E-mail: xgx2014@tsinghua.edu.cn; Jianbin LUO, E-mail: luojb@tsinghua.edu.cn

materials, making the surfaces corrosion-resistant, self-cleaning, self-healing, and water/oil releasing [1]. Moreover, polymer coatings with low shear strengths have good self-lubricity and wear resistance, and can provide extremely low coefficients of friction and wear under specific or highly controlled test conditions. Self-lubricating polymer coatings have a combination of properties that are not found in other solid lubricating coatings, and they are particularly favored in applications where cost, weight, corrosion resistance, and biocompatibility are significant considerations [2].

However, self-lubricating polymer coatings have many limitations. Compared with hard coatings such as ceramic coatings and carbon-based coatings, they have weak wear resistance, more wear debris, and a more limited life. Low thermal conductivity and poor heat resistance make it easy for the coatings to soften and fail at high temperatures. Moreover, their tribological performance is strongly dependent on the environment. A worn surface may exhibit different chemistries, microstructures, and crystallographic textures from the overall coating owing to the surface chemical reaction with the surrounding environment. Extremely low friction and long wear life produced in one environment may not be possible in another environment [3]. Degradation associated with oxidation and aging is also an obstacle for some applications. Combining materials with different properties is an effective method for enhancing material properties by fully exploiting the advantages of two or more components, and the properties of materials can be tailored and optimized. Therefore, functional fillers have been utilized to improve the performance of polymer coatings, including providing a stable and low coefficient of friction, high thermal conductivity and heat resistance, enhanced mechanical properties for higher loads, and optimized adhesion between the coating and substrate.

This review focuses on the analysis of the tribological properties, mechanical properties, and adhesion properties of self-lubricating polymer composite coatings. First, the matrices, fillers, and coating preparation methods of polymer composite coatings are introduced in Section 2 (Polymer composite coatings). Second, the tribological properties of polymer composite coatings with different matrices and fillers are compared, and the lubrication mechanisms are discussed in Section 3 (Tribological properties of polymer composite coatings). The strengthening and toughening mechanisms of polymer composite coatings are summarized in Section 4 (Mechanical properties of polymer composite coatings). Next, the methods for detecting the adhesion strength between polymer composite coatings and substrates and enhancing coating adhesion are described in Section 5 (Adhesion properties of polymer composite coatings). This paper provides the basis for the selection, design, and use of polymer coating systems, and finally points out the deficiencies and disadvantages of current polymer composite coating research in Section 6 (Summary and outlook).

2 Polymer composite coatings

Figure 1 shows an overview of conventional polymer matrices, classification of fillers, and specific filler materials. In reviewing the literature, the common polymer materials used as lubrication coating matrices include epoxy resin (EP), phenolic resin (PF), aromatic thermosetting copolyester (ATSP), polyp-hydroxybenzoic acid (PHBA), polyimide (PI), polyamide-imide (PAI), polyurethane (PU), polyamide (PA), polyethere-therketone (PEEK), polytetrafluorethylene (PTFE), ultra-high molecular weight polyethylene (UHMWPE), polyphenylene sulfide (PPS), and polyoxymethylene (POM). However, a single polymer as a lubrication coating always has certain constraints in application. For example, although PTFE [4] has excellent chemical inertness, thermal stability, and an ultra-low coefficient of friction, it creeps easily and has a high wear rate under high loads. PI [5] is a high-performance engineering plastic with high-temperature resistance properties, excellent mechanical properties, and high creep resistance,

but its high friction coefficient restricts its application in lubrication. PPS [6] has good high-temperature resistance. At the same time, it has excellent corrosion resistance, radiation resistance, and chemical resistance, but its inherent brittleness and low impact strength make it unsuitable for applications in harsh working conditions, such as bearings and sliding parts. Other materials such as fillers are added to improve the tribological and mechanical properties to address the limitations of single polymer materials. The materials used as fillers can be roughly divided into six types: carbon-based materials, transition metal sulfides, polymers, ceramic nanoparticles, soft metals, mineral silicon salts, and microcapsules.

2.1 Polymer matrix

Lubrication coatings are mainly applied to reduce the friction and wear of mechanical parts, which improves the equipment performance and service life. Strict requirements for the coating's performance are based on the service conditions, including high temperature, high pressure, high speed, vacuum, and radiation. Therefore, the actual working conditions must be considered when selecting a suitable polymer as a matrix.

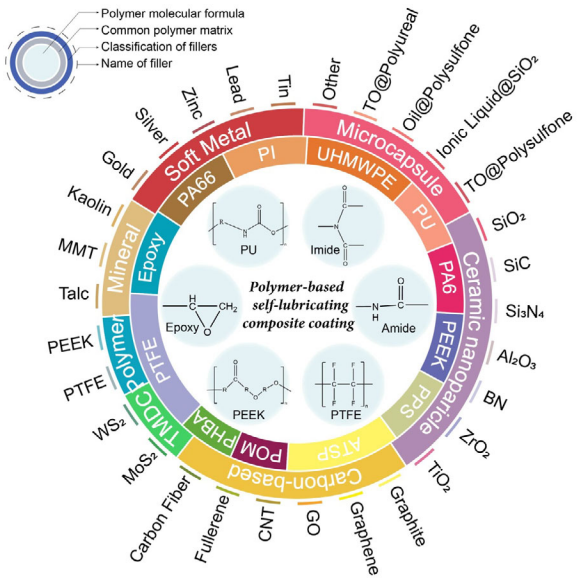

Fig. 1 Common matrices and fillers of polymer composite coating.

Temperature resistance is one of the essential properties of polymer coatings that must be considered. During repetitive and continuous motion, the temperature rise is unavoidable, which leads to a sharp degradation of the material properties and further causes the failure of the coating. In addition, excellent mechanical properties are needed to meet high-load and high-speed conditions. Moreover, chemical resistance allows the coating to adapt to a variety of working environments, such as acidic or alkaline atmospheres. As a self-lubricating coating, the primary role is to reduce the friction coefficient between friction pairs and reduce the wear rate of the substrates; therefore, the friction coefficient of polymer materials is a valuable property that needs to be considered. Table 1 presents the summary data of the glass transition temperature (T_g), melting temperature (T_m), maximum continuous service temperature (T_s), tensile strength, Young's modulus, chemical resistance, and coefficient of friction (COF) of common polymer materials.

Based on the data in Table 1, Fig. 2 compares the performance of different polymers more intuitively. The heat resistance of polymer coatings is mainly characterized by the maximum continuous service temperature, which is closely related to the glass transition temperature. Figure 2(a) compares the glass transition temperature and the maximum continuous service temperature of common polymer matrices. As can be seen from Fig. 2(a), the heat resistance of PAI, PI, ATSP, PEEK, and PPS is superior, and the maximum continuous service temperature is approximately 250 °C. The heat resistance of PA66 and UHMWPE is relatively poor. The tensile strength and elastic modulus of the polymer materials are compared in Fig. 2(b). Polymer materials with excellent heat resistance also have strong mechanical properties, such as PAI, PI, and PEEK. Figure 2(c) shows the friction coefficient of the polymers, and indicates that UHMWPE, POM, PTFE, and PAI have outstanding self-lubricity. Although PI and ATSP have excellent heat resistance and mechanical properties, their friction coefficients are high.

Table 1 Properties of common polymer matrices.

Materials	$T_g/T_m/T_s$ (℃)	Mechanical properties		Chemical resistance	COF
		Tensile strength (MPa)	Young's modulus (GPa)		
EP	50–80/*/120 [7]	52.98 [8]	3.15 [8]	Good	0.6–0.7 [9, 10]
PF	240 [11]/*/260 [12]	53.2 [13]	7 [13]	Good	0.42 [14]
ATSP	240 [15]/*/260 [16]	88 [17]	4.35 [17]	Good	0.22 [16]
PU	–42/168 [18]/85 [19]	24.8 [20]	57.8 [20]	Fair	0.34 [21]
PI	212 [22]/375/221 [23]	101 [24]	1.9 [24]	Good	0.49 [25]
PTFE	125/327 [26]/260 [19]	33 [27]	0.27 [27]	Good	0.07–0.1 [28, 29]
PA66	75/263 [30]/140 [31]	80 [32]	2.41 [32]	Only alkali	0.44 [33]
PA6	59/224 [34]/120 [31]	68 [35]	3.4 [35]	Only alkali	0.41 [36]
PAI	277 [37]/*/260 [38]	138 [39]	4.1 [39]	Only alkali	0.2 [40]
PEEK	143/340 [41]/260 [42]	90 [43]	3.0 [43]	Good	0.3–0.4 [44, 45]
UHMWPE	–133 [46]/135 [47]/90 [19]	32.8 [48]	0.6 [48]	Good	0.10–0.16 [49, 50]
PPS	85 [51]/286 [52]/220 [53]	78 [54]	2.5 [54]	Good	0.45 [55]
POM	–60/170 [56]/120 [57]	55.5 [58]	2.65 [58]	Poor	0.3–0.33 [59, 60]

Note: * means the polymer has no melting temperature.

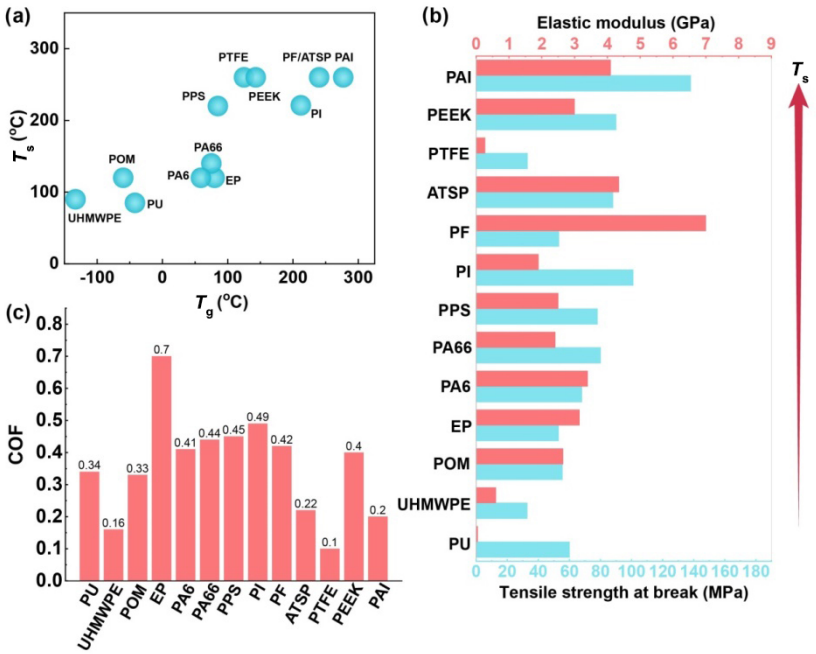

Fig. 2 Comparison of (a) heat resistance, (b) mechanical properties, and (c) friction coefficient of common polymer matrices.

2.2 Functional fillers

Types of fillers can be classified into reinforcing fillers and lubricating fillers, according to their functions. Reinforcing fillers are materials with a higher strength and modulus than the matrices, which can enhance the mechanical properties of polymer composites. Fibers and nanoparticles are employed as reinforcing fillers in a considerable amount of the literature. Conventional reinforcing fibers include carbon fibers, glass fibers, and silicon fibers [61, 62]. In addition, carbon nanotubes are also excellent for reinforcing polymer composite materials because of their one-dimensional structure, similar to fibers, and high strength [61, 63]. Two-dimensional nanoclays,

such as montmorillonite, are also widely used to enhance the mechanical properties of polymer materials [64].

Moreover, almost all types of nanoparticles can be used as a reinforcement phase for polymer-based composites, including Al_2O_3, SiO_2, ZnO, SiC, and Cu. Lubricating fillers can be defined as functional materials that reduce the friction coefficient of polymer composite materials. Lubricating fillers mainly include polytetrafluorethylene, graphite, graphene, molybdenum disulfide, black phosphorus, gold, and copper [65–67]. Some reinforcing fillers can effectively improve the friction properties of polymers while enhancing their mechanical properties. For example, the addition of silica and short carbon fibers to an epoxy resin effectively improves the friction properties of the resin [68]. Carbon nanotubes have been used to improve the tribological properties of PA6 [69]. In addition, the rolling bearing effect of nanoparticles in the friction process can also effectively reduce the friction coefficient [70]. Likewise, high-strength lubricating fillers such as graphite and graphene can also enhance the mechanical properties of polymers [71].

The classifications and properties of the fillers are introduced in this section. According to previous reviews, carbon nanomaterials have attracted great interest for their confirmed friction reduction and anti-wear performance, as well as important tribological applications. Four typical carbon nanomaterials, including fullerenes, graphene, carbon nanotubes (CNTs), and nanodiamonds, have been applied in coatings for anti-wear enhancement and friction reduction [72, 73]. Fullerene is a graphene-based material, with large carbon cage molecules considered to be zero-dimensional (0D) analogs of benzene. Its lubricating behavior is of great interest because of its spherical shape, strong intramolecular nature, and weak intermolecular bonding [74]. Graphene has excellent strength and good toughness, with a Young's modulus of 1 TPa and tensile strength of up to 100 GPa [75, 76]. Its layered structure promotes good lubrication, so it is widely used to enhance the tribological and mechanical properties of a polymer matrix [74]. Carbon fibers (CF) [55] and carbon nanotubes (CNTs) [77] are also used as reinforcing fillers owing to their excellent mechanical properties. Nanodiamonds show very low surface roughness and excellent mechanical properties, which play a key role in the friction and wear behaviors of self-mated tribosystems [78, 79]. In addition, black phosphorus is an emerging two-dimensional lubricating and reinforcing filler, which will be discussed later. Transition metal sulfides, mainly molybdenum disulfide (MoS_2) and tungsten disulfide (WS_2), are good lubricants for reducing the friction coefficient and wear rate of the polymer matrix because of their layered structure [80, 81]. Mineral silicon salts, such as montmorillonite and kaolin, have a lamellar structure with a high aspect ratio and large interfacial area that can be cross-linked with polymers to enhance the stiffness and creep resistance of the polymer matrix [64, 82, 83]. Soft metals, including gold, silver, and tin, can easily form films and each has a high thermal conductivity, making them suitable as lubricants for high-temperature conditions [84–86]. Ceramic nanoparticles, including silicon dioxide (SiO_2), silicon carbide (SiC), silicon nitride (Si_3N_4), aluminum oxide (Al_2O_3), and titanium dioxide (TiO_2), can maintain superior mechanical properties at room and high temperatures. Therefore, they are usually applied as a reinforcing phase to improve the mechanical properties and wear resistance of polymer materials [70, 87–91].

In general, liquid lubricants are far superior to solid lubricants for improving the lubricating performance of materials, and the coefficient of friction for liquids can even be lower by 1–2 orders of magnitude than that of solid lubricants. However, the replenishment, storage, and retention of lubricating oil on the material surface during the friction process remains a significant limitation to its application. Microcapsules effectively combine the advantages of solid lubrication and liquid lubrication, where the polymer or inorganic substance is used as the shell layer, and the liquid lubricant is encapsulated inside the shell as the capsule core. When the shell is broken under pressure or shear force, the internal liquid lubricant is released, and a liquid lubricating film is formed on the contact surface.

Commonly used microcapsule shell materials include polymelamine formaldehyde (PMF), polysulfone (PSF) [92], polyuria (SPUA) [93], and silica [94]. Organic and inorganic substances can act as shell layers collaboratively, such as polystyrene and silicon dioxide [95]. The core liquid lubricants include mineral oil [95], ionic liquid [94], tung oil [92], and the like.

2.3 Preparation methods

Preparation methods of solid lubricating coatings significantly affect the coating properties. A number of techniques have been developed to prepare non-polymer solid lubricant coatings, such as diamond-like carbon and metal alloy coatings, including magnetron sputtering, electroplating, electroless plating, plasma-assisted chemical vapor deposition, physical vapor deposition, pulsed laser deposition, and vacuum deposition [3]. However, these methods are not suitable for polymer coatings in most cases. A systematic literature review was conducted on polymer lubrication coatings. Various methods, including brush coating, roller coating [96], dip coating, flow coating, spin coating [97], spray coating (air/thermal/cold/electrostatic) [98, 99], hot-press sintering, plasma polymerization, grafting, and laser deposition have been employed to fabricate polymer composite coatings. Figure 3 presents the various methods for preparing polymer coatings. As shown in Fig. 3, brush coating, roller coating, dip coating, spin coating, and partial spraying require dissolving the polymer in suitable volatile solvents. Then the polymer solution is applied on the substrate and the coating forms following the evaporation of the solvents. Commonly used solvents are aliphatic and aromatic hydrocarbons, alcohols, esters, ketones, and chlorinated solvents, which cause environmental pollution and need to be recaptured. Moreover, the recapturing processes become extremely harmful, expensive, and difficult to handle. However, thermal spray, cold spray, and powder electrostatic spray avoid this disadvantage because the paint is in powder form. Table 2 introduces the characteristics of the polymer coating preparation methods, including the applicable substrate, state of the feedstock, factors affecting the coating quality, and each methods' strengths and weaknesses.

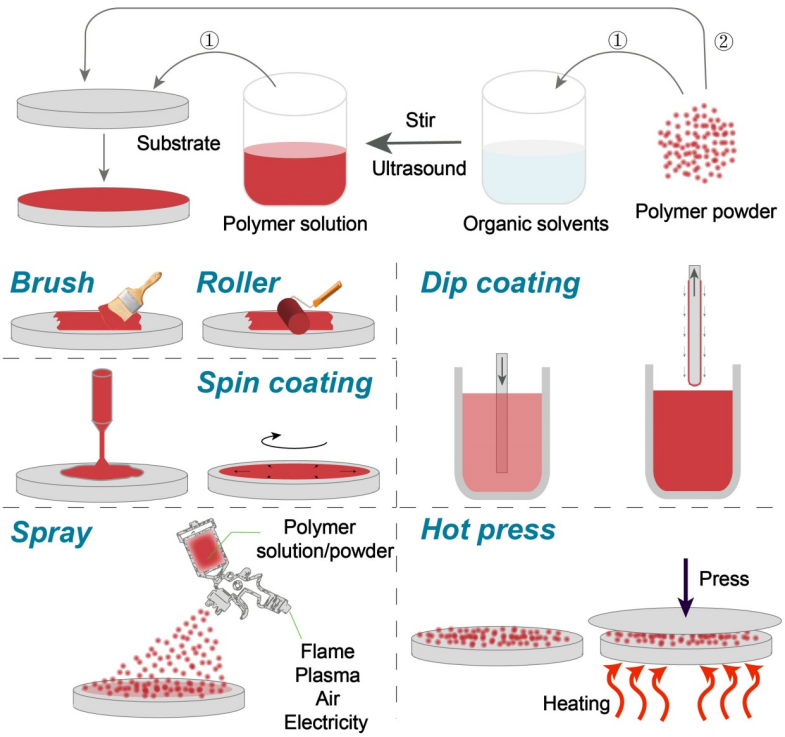

Fig. 3 Schematic diagram of various methods for preparing polymer coatings.

Table 2 Comparison of polymer coating preparation methods.

Methods	Substrate	Feedstock	Factors affecting coating quality	Strengths and weaknesses
Brush/ roller coating	Any substrate	Solution	Substrates surface quality Manual skill	✓ Better wetting, suitable for small area, less waste and pollution × Low efficiency, uneven coating thickness, and poor repeatability
Dip coating	Any substrate	Solution	Viscosity, density, surface tension, concentration, immersion time, extraction speed, number of cycles, substrate properties	✓ Simple, scalable, fast, low cost, suitable for large-scale preparation of uniform coatings × Poor adhesion
Spin coating	Any substrate	Solution	Molecular weight, concentration, viscosity, solvent evaporation rate, solvent diffusivity, volatility, rotational angular velocity	✓ Short preparation time, uniform thickness and low equipment cost × Substrate size limited by equipment and only suitable for flat substrates
Air spray	Any substrate	Solution	Solution viscosity, spray gun pressure, spray distance and angle	✓ Suitable for large area substrate, uniform coating × High equipment requirements and low coating deposition efficiency
Electro-static spray	Any substrate	Solution Powder	Spray voltage and current, the rest is the same as air spray	✓ Uniform coating, strong adhesion, high coating deposition efficiency and high coverage × Paints need good conductivity, expensive equipment, high voltage danger
Thermal spray	Non-polymer	Powder	Spray particle temperature, particle speed, spray angle and distance, particle size, filling method, substrate temperature, surface quality, roughness, substrate cooling rate	✓ The paint is powder, no volatile pollution, eliminating the need for expensive solvent treatment, not limited by the melt viscosity and thermal conductivity of the substrate, high deposition efficiency × Noisy, not suitable for polymer substrates, problems such as oxidation, evaporation, degumming, residual stress, gas release of materials are inevitable
Cold spray	Any substrate	Powder	Particle speed (greater than critical speed), others are the same as thermal spraying	✓ Suitable for a variety of substrates, avoiding the disadvantages of thermal spraying, and good coating adhesion × Large equipment, unstable process and low powder utilization rate
Hot press sintering	Non-polymer	Powder	Sintering temperature, pressure, time	✓ Simple and low equipment cost × Not suitable for large area coatings

Extensive research has shown that the morphologies of the coatings are significantly influenced by the preparation methods and processing parameters. Na et al. [100] systematically characterized the effects of spin-coating time on the microstructural evolution. The surface topography, structure, and surface roughness of the films vary widely with various spin coating times. Nanoscale aggregated features appear when the spin-coating time is long, and nanofibrillar network structures are evident in the film with a short spin-coating time. The root-mean-square surface roughness values of the thin films tend to increase at shorter spinning times. In the spin-coating process of the polymer and fullerene bulk-heterojunction blend, solvent evaporation rate changes cause a lateral phase separation gradient, and the roughness decreases as it moves away from the center of rotation [101]. Using the same coating preparation method, the morphologies of coatings with different polymer types and the concentration ratio of different polymer mixture components varied greatly [102, 103]. The characteristics of the feedstock, such as the type of solvent, polymer molecular weight, and polymer concentration, are also important factors affecting the coating morphology. Dário et al. [104]

found that the void content of polymer films increased with the acetone content in the solvent mixture and decreased with increasing polymer molecular weight. In the polystyrene (PS)/ polymethylmethacrylate (PMMA) blend film, with an increase in the molecular weight of the polystyrene, three different types of surface morphologies were observed, namely nanophase separation morphology, network morphology, and island-like morphology [105]. The phase separation morphology was also observed in polydimethylsiloxane (PDMS)/polystyrene and polyphenylsilsequioxane (PPSQ)/polystyrene blends. Types of silicon-containing constituents, polymer blend composition, concentration of the polymer blend solution, surface tension of the substrate, and spin-coating speed can affect the ultimate morphologies of phase separation [106]. Cui et al. [107] studied the effects of polymer concentration. Continuous films, net-like structures, and droplets were found for polystyrene (PS) with a decrease in concentration. Petri [108] reported the relationship between the morphology and the competitive interactions between the polymer, solvent, and substrate. When the interaction energy between the substrate and the solvent overcomes that between the substrate and the polymer, the film becomes rough and segregates. In contrast, when the interaction energy between the substrate and the polymer is stronger than that between the substrate and the solvent, or when both interaction energies are weak, the film is homogeneous and flat.

In addition to the well-known parameters, the morphologies of polymers are strongly influenced by the wettability of the substrate [109]. The morphologies of the coatings prepared by dip-coating are also closely related to the process parameters. Various morphologies such as layered films and laterally phase-separated domains could be formed depending on the deposition parameters (withdrawal speed and geometry of the reservoir) [110]. Jiang et al. [111] studied polydopamine (pDA)-coated polymer films and found that surface roughness is mainly affected by the reaction temperature. van Stam et al. [112] comparatively studied the morphology of polyfluorene: Fullerene films prepared through spin coating and dip coating. Similar morphological structures can be obtained by the two preparation methods, and the final film morphology can be controlled by appropriately selecting the dip-coating speed. Dip coating provides more possibilities for controlling the morphology of the film.

The morphology of thermal spray coatings is related to the process parameters mentioned in Table 2. By optimizing the process parameters, high-quality coatings can be obtained. Polyvinylidene fluoride (PVDF), ethylene chlorotrifluoroethylene (ECTFE), perfluoroalkoxy alkane (PFA), and fluorinated perfluoroethylene (FEP) coatings are produced by flame and plasma spraying processes. The spray coating was found to be non-porous and very smooth [113]. UHMWPE/graphene nanosheet coatings were deposited by flame spraying. The coatings achieved a dense microstructure without cracks or other surface defects, and no visible holes or inclusions were found in the coating [114]. By simultaneously injecting powder into a plasma jet, alumina, magnesium hydroxide, silica, and stainless steel are co-deposited with nylon. Dense deposited films with a strong bond between the filler particles and the matrix are produced. Furthermore, different fillers lead to different coating morphologies [115]. Nano-silica and carbon-black-filled nylon 11 coatings are successfully sprayed using the high-velocity oxy-fuel (HVOF) combustion spray process. The morphology of the polymer and the microstructure of the coating depends on the surface chemistry of the filler and the volume fraction of the filler, as well as the initial particle size of nylon 11. Coatings made from smaller polymer particle sizes show an improved spatial distribution of silica in the matrix and lower crystallinity. In addition, coatings made from smaller polymer particles have lower porosities [116]. The cold spray deposition of polyurethane, polystyrene, polyamide 12, and ultrahigh molecular weight polyethylene are very similar, with almost no pores, a smooth surface, and no obvious traces of powder [117].

Many investigators have also examined the effects of the morphologies of coatings on tribological and mechanical properties. The main surface morphology

characteristics affecting tribological properties are surface roughness and texture patterns. Baum et al. [118] prepared epoxy samples with different surface structures, including periodical groove-like surfaces, random roughness surfaces, snake-inspired microstructured surfaces, and smooth surfaces. Compared to a smooth surface, snake-inspired microstructured surfaces and random roughness surfaces have lower coefficient of friction. The snake-inspired microstructure leads to a more significant reduction in the friction coefficient and an anisotropic friction characteristic. Moreover, the stick–slip phenomenon during sliding is also reduced. Song et al. [119] investigated the effect of roughness on the tribological properties of polyimide composites. The friction coefficient and wear rate of polyimide composites increase with an increase in surface roughness. Moreover, the crystallinity of the polymer can significantly affect the mechanical properties and friction properties of the polymer. In another study, semi-crystalline PEEK coating has a higher hardness than an amorphous PEEK coating, and the dispersed spherulites in the amorphous matrix limit the movement and slippage of the polymer chain, thereby increasing the stiffness of the coating. Obvious plastic deformation and severe plow marks were observed on the worn surface of the amorphous coating. For semi-crystalline coatings, plastic deformation is reduced, and a relatively smooth worn surface is observed. The above results showed that the crystallinity of PEEK enhanced the tribological properties [120].

3 Tribological properties of polymer composite coatings

Polymer composite coatings are mainly applied to control the friction and wear of friction pairs. A large and growing body of literature has investigated the tribological properties of polymer composite coatings. Different theories exist in the literature regarding the lubrication mechanisms of polymer coatings, and they focus on the formation of a transfer film on the lubricated surfaces. The composition, structure, and properties of the transfer film have been identified as significant factors determining the friction and wear characteristics of polymer materials [121−124]. Combining functional nanoparticles with polymers can significantly enhance the tribological performance of PEEK reinforced with carbon fibers. Also, the addition of the fillers can accelerate the formation speed of the transfer film [125]. This section systematically reviews and aims to provide a depth of understanding of the tribological properties of polymer coatings. The substrates, fillers, preparation methods, thicknesses, and main tribological performance parameters (friction coefficient and wear rate) of the typical polymer composite coatings reported so far are summarized in Table 3. Using the minimum friction coefficient and corresponding wear rate data of different composite coatings in Table 3, the friction performance is compared by plotting the friction coefficient as a function of wear rate in Fig. 4.

Figure 4 indicates that the tribological properties of the composite coatings show an obvious correlation with the types of polymer matrix. The epoxy-based composite coating has a low wear rate, but its friction coefficient is relatively high. In contrast, the PTFE-based composite coating has a low friction coefficient, whose minimum is approximately 0.05, but its wear rate is higher than that of the epoxy-based coating. The PTFE composite coating has a relatively low coefficient of friction because its matrix PTFE has excellent self-lubricating properties. PTFE is composed of carbon and fluorine atoms that form strong chemical bonds, and the fluorocarbon molecules are structured such that the fluorine atoms surround the carbon atoms. With the fluorine atoms running helically on the surface, the PTFE chain resembles a rigid, cylindrical rod with a smooth surface. The low friction coefficient of PTFE is closely related to the smooth profile of the rigid rod-shaped PTFE molecules. Owing to the severe mechanical stresses and thermal vibrations associated with frictional heating, the PTFE's molecular chain fractures into chain fragments by breaking −C−C− and/or−C−F− bonds. The active PTFE radicals (chain fragments) and the fluorine ions react and chemically bond with the metallic elements of the counterface, which results in strong adhesion and

Table 3 Friction properties of typical polymer composite coatings.

Matrix	Filler	Substrate	Methods	Thickness	Steady state friction coefficient	Ear rate/life
Epoxy	KH550- Fullerene [74]	Cast iron	Brush	250 μm	0.68 (0 wt%)−0.6 (0.5 wt%) (3 N，0.01 m/s) 316L steel	0.006 (0 wt%)−0.002 (0.5 wt%) mm^2
	KH550- fullerene [74]	Cast iron	Brush	250 μm	0.68 (0 wt%)−0.6 (0.5 wt%) (3 N，0.01 m/s) 316L steel	0.006 (0 wt%)−0.003 (0.5 wt%) mm^2
	Graphene (G) [154]	Gcr15 steel	Spray	30 μm	0.60 (0 wt%)−0.11 (4 wt%) (4 N, 0.072 m/s) Gcr15 steel	6.54 (0 wt%)−1.0 (4 wt%) $\times10^{-6}$ $mm^3/(N·m)$
	Carbon nanotubes / zinc sulfide [77]	Steel	Spray	—	0.76 (0 wt%)−0.42 (1.25 wt%) (1.5 N, 200 rpm) Gcr 15steel	19 (0 wt%)−1 (1.25 wt%) $\times10^{-4}$ $mm^3/(N·m)$
	Graphite (GP) [157]	Tinplate	—	—	0.56 (0 wt%)−0.32 (50 wt%) (25 N, 0.84 m/s) 45 steel	27 (0 wt%)−18 (50 wt%) $\times10^{-11}$ $mm^3/(N·m)$
	Tung oil @ polysulfone capsules (TO@PUF) [92]	Steel	—	200 μm	0.46 (0 wt%)−0.35 (10 wt%) (1.0 MPa, 0.51 m/s) stainless steel	38.64 (0 wt%)−13.10 (10 wt%)$\times10^{-14}$ $m^3/(N·m)$
	Tung oil @ polyureal capsules (TO@PUF) [93]	Steel	—	300 μm	0.46 (0 wt%)−0.38 (10 wt%) (1.0 MPa, 0.51 m/s) stainless steel	38.64 (0 wt%)−8.26 (10 wt%)$\times10^{-14}$ $m^3/(N·m)$
	70SN Lubricant @ PS/SiO_2 cpsule ($O@PS/SiO_2$) [95]	Aluminum	—	—	0.57 (0 wt%)−0.27(10 wt%) (1.0 MPa, 0.51 m/s) steel	3.86 (0 wt%)−0.273 (10 wt%) $\times10^{-13}m^3/(N·m)$
	Oily diatomite [158]	Steel	Electrostatic spray	250 ±10 μm	0.59 (0 wt%)−0.095 (16 wt%) (2.0 MPa, 0.76 m/s) steel	0.088 (0 wt%)−0.0014 (16 wt%) g/h

Matrix	Filler	Substrate	Methods	Thickness	Steady state friction coefficient	Wear rate/life
	30 wt% polyfluo-wax graphite [159]	45 steel	Spray	60−70 μm	0.179 (0 wt%)−0.201 (30 wt%G) (320 N, 2.56 m/s); 0.187 (320 N) −0.1 (720 N) (10 wt%, 2.56 m/s); 0.24 (1.28 m/s)−0.14 (3.84 m/s) (10 wt%, 320 N)	675 (0 wt%)−1,700 (10 wt%); 1,700 (320 N)−200 (720 N); 1,700 (2.56 m/s)−450 (3.84 m/s) m/μm
Phenolic resin	30 wt% polyfluo-wax MoS_2 [159]	45 steel	Spray	60−70 μm	0.179 (0 wt%)−0.202 (40 wt%G) (320 N, 2.56 m/s); 0.182 (320 N)−0.12 (720 N) (10 wt%, 2.56 m/s); 0.22 (1.28 m/s)−0.16 (3.84 m/s) (10 wt%, 320 N)	675 (0 wt%)−300 (50 wt%); 450 (320 N)−150 (720 N); 450 (2.56 m/s)−150 (3.84 m/s) m/μm
	20 wt% polyfluo-wax graphene [160]	45 steel	Spray	—	0.179 (0 wt%)−0.125 (0.3 wt%) (320 N, 2.24 m/s); 0.125 (320 N)−0.100(620 N) (0.3 wt%, 2.24 m/s); 0.14 (2.24 m/s)−0.13 (3.68 m/s) (0.3 wt%, 320 N) steel	400 (0 wt%)−4,000 (0.3 wt%);4,000 (320 N)−600 (620 N); 4,000 (2.24 m/s)−2,000 (3.68 m/s) m/μm
	Carbon fiber [55]	45 steel	Flame spray	250−350 μm	0.45 (0 wt%)−0.4 (5 wt%) (200 N, 0.43 m/s) stainless steel	8 (0 wt%)−19 (5 wt%) $\times 10^{-6} mm^3/(N \cdot m)$
Polyphenyl ene sulfide	30 wt% polyfluo-wax Graphene [6]	45 steel	Spray	50 μm	—(100 N, 0.43m/s) GCr steel	5 (0 wt%)−50(5 wt%)m/μm
	PTFE [133]	Steel	Spray	40−50 μm	0.36 (0 vol%)−0.18 (40 vol%) (320 N, 1.25 m/s); 0.18−0.15 (320−700 N)0.2−0.15 (0.75-2.5 m/s) steel	230 (40 vol%);230−25; 240−60 m/μm
PHBA	PA66 MoS_2 [161]	45 steel	Brush	20−40 μm	0.043 (150 (Kpa·m)/s)−0.033 (1,800 (Kpa·m)/s)（20 wt% PA66, 30 wt% MoS2）steel	2×10^{-6} $mm^3/(N \cdot m)$

Matrix	Filler	Substrate	Methods	Thickness	Steady state friction coefficient	Wear rate/life
	30 wt% polyfluo-wax TDI-carbon nanotubes [156]	45 steel	Spray	50−60 μm	0.171 (0 wt%)−0.225 (3 wt%) (320 N, 2.56 m/s); 0.20 (320 N)−0.13 (520 N) (1 wt%, 2.56 m/s); 0.202 (1.28 m/s)−0.185 (3 m/s) (10 wt%,320 N) steel	700 (0 wt%0−1,800 (3 wt%); 1,500 (320 N)−900 (620 N); 500 (0.64 m/s)−1,800 (3 m/s); m/μm
	30 wt% polyfluo-wax silica [91]	Steel	Spray	30−40 μm	0.17 (0 wt%)−0.14 (1 wt%) (320 N, 2.56 m/s); 0.16 (320 N)−0.07 (820 N) (3 wt%, 2.56 m/s); 0.20 (0.64 m/s)−0.16 (3.84 m/s) (3 wt%, 320 N) steel	300 (0 wt%)−750 (3 wt%); 750 (320 N)−500 (820 N); 500 (0.64 m/s)−1,000 (3.84 m/s); m/μm
	30 wt% polyfluo-wax HDI-titanium dioxide nanotubes (TiNT) [155]	Steel	Spray	30−50 μm	0.135 (320 N)−0.05 (1,620 N) (1 wt%, 2.56 m/s); 0.20 (1.28 m/s)−0.13 (3.84 m/s) (1 wt%, 320 N) steel	2,750 (320 N)−1,000 (1,620 N); 2,750 (2.56 m/s)−2,500 (3.84 m/s); m/μm
Polyurethane	20 wt% polyfluo-wax ionic liquid @ SiO2 capsule [94]	Steel	Spray	40−50 μm	0.20 (0 wt%)−0.09 (20 wt%) (3 N, 2.5 cm/s); 0.09 (3 N)−0.05 (10 N) (20 wt%, 2.5 cm/s) GCr15 steel	500 (0 wt%)−200 (wt%); 170 (3 N) −550 (10 N); μm
	30 wt% polyfluo-wax silicon carbide [70]	45 steel	Spray	40−50 μm	0.172 (0 wt%)−0.133 (5 wt%) (320 N, 2.56 m/s); 0.13 (320 N)−0.06 (820 N) (5 wt%, 2.56 m/s); 0.23 (0.64 m/s)−0.14 (3.84 m/s) (5 wt%, 320 N) steel	300 (0 wt%)−600 (5 wt%); 600 (320 N) −500 (820 N); 200 (0.64 m/s) −800 (2.0 m/s); m/μm
	30 wt% polyfluo-wax zirconia (GrO) [70]	45 steel	Spray	40−50 μm	0.172 (0 wt%)−0.137(1 wt%) (320 N, 2.56 m/s); 0.15 (320 N)−0.05 (820 N) (5 wt%, 2.56 m/s); 0.23(0.64 m/s)−0.12 (3.84 m/s) (5 wt%, 320 N) steel	300 (0 wt%)−1,000 (5 wt%); 1,500 (420 N)−450 (820 N); 4,00 (0.64 m/s) −1,000 (2.56 m/s); m/μm
	PTFE [21]	Babbitt	Spray	8−10 μm	0.34 (0 wt%)−0.15 (7 wt%)(3.08 MPa,0.08 m/s) GCr15 steel	2.03 (0 wt%)−1.35 (3 wt%) $\times 10^{-4}$ mm^3/(N·m)

Matrix	Filler	Substrate	Methods	Thickness	Steady state friction coefficient	Wear rate/life
Polyimide	MoS2@HCNT [5]	Steel	Solution cast	50 μm	0.4 (0 wt%)−0.35 (2.0 wt%) (20 N, 12 cm/s) GCcr15steel	1.5 (0 wt%)−0.75 (0.5 wt%) $\times 10^{-6}$ mm^3/(N·m)
	Fluorinated graphene (FG) [162]	Steel	Solution cast	100 μm	0.39 (0 wt%)−0.36 (0.25 wt%) steel	1.5 (0 wt%)−0.8(0.5 wt%) $\times 10^{-5}$ mm^3/(N·m)
	PTFE silicon nitride [132]	45 steel	Spray	—	0.346 (pure), 0.149 (20 PTFE), 0.140 (20 PTFE, 5Si_3N_4) (4 N, 0.33 m/s); 0.140−0.123 (4−10N, 0.33 m/s); 0.117−0.130 (0.11−0.77 m/s, 8 N) Gcr15 steel	2.736, 1.313, 0.244; 0.244−0.1; 0.65−0.55; $\times 10^{-4}$ mm^3/(N·m)
	L-phenylalanine -graphene (LG) [25]	Steel	Solution cast	50 μm	0.49 (0 wt%)−0.44 (0.6 wt%) (3 N, 2 Hz) steel	3.9−0.82$\times 10^{-5}$ mm^3/(N·m)
	Fullerene (C_{60}) [163]	Steel	Solution cast	150−200 μm	0.25 (10 N, 1 m/s) steel	15−1$\times 10^{-7}$ mm^3/(N·m)
	Boron nitride(BN), silicon nitride, perfluoropolyether(PFPE), platelets(Lapis) [164]	Steel	Spray	29 μm	0.06 (2 N, 10 mm/s) steel	>1,000 cycles
Polyamideimide	Oligomeric silsesquioxane (POSS)-MoS_2 [137]	Steel	Spray	25 μm	0.09 (50 wt% MoS_2); 0.085 (5 wt% OPSS); 0.08 (5 wt% OMPOSS) (10 N, 100 mm/s)	7; 3;2$\times 10^{-6}$ mm^3/(N·m)
	Oligomeric silsesquioxane (POSS)-PTFE [134]	Steel	Spray	25−30 μm	0.073 (0 wt%)−0.057 (7 wt%) (5 N, 0.1 m/s) steel	6.5 (0 wt%)−3.4 (7 wt%) $\times 10^{-6}$ mm^3/(N·m)

Matrix	Filler	Substrate	Methods	Thickness	Steady state friction coefficient	Wear rate/life
Polyamide	Graphene [138]	45 steel	Flame spray	250−350 μm	0.33 (0 wt%)−0.15 (1 wt%) (200 N, 0.43 m/s); steel	6.5 (0 wt%)−3.5 (5 wt%) $\times 10^{-4}$ mm^6/(N·m)
	MoS_2 [138]	45 steel	Flame spray	250−350 μm	0.33 (0 wt%)−0.23 (7 wt%) (200 N, 0.43 m/s) steel	20 (0 wt%)−10 (1 wt%) $\times 10^{-6}$ mm^3/(N·m)
	Alumina [138]	45 steel	Flame spray	250−350 μm	0.33 (0 wt%)−0.23 (10 wt%) (100 N, 0.43 m/s) steel	6.5 (0 wt%)−3.5 (0.5 wt%) $\times 10^{-4}$ mm^3/(N·m)
Polyetheretherketone	Silicon carbide [44]	Aluminum	Brush	40 μm	0.31−0.20 (0 wt%, 1 N, 0.2−1.4 m/s); 0.29−0.36 (0 wt%, 9 N, 0.2−1.1 m/s); 0.36−0.42 (7 wt%, 1 N, 0.2−0.8 m/s); 0.35−0.25 (7 wt%, 9 N, 0.2−1.4 m/s) steel	20−75 (0 wt%,); 25−150 (0 wt%); 10−25 (7 wt%); 30-60 (7 wt%)$\times 10^{-6}$ mm^3/N·m
	Silica [165]	Steel	Electrostatic spray	150 μm	0.35 (0 vol%)0−0.37 (15 vol%) (3N, 0.13 m/s); 0.37−0.46 (3 N−11 N, 0.13 m/s) steel	27−21; 21−40 $\times 10^{-6}$ mm^3/(N·m)
	Non-polar fullerene tungsten disulfide [45]	Steel	Spray	30 μm	0.4 (0 wt%)−0.15 (2.5 wt%) (1 N, 30 mm/s) steel	—
	PTFE [135]	Cast iron	Spray	20−25 μm	0.077 (5 wt%, 445 N, 3.6 m/s)	8.50$\times 10^{-7}$ mm^3/(N·m)
ATSP	Graphene [136]	Steel	Electrostatic spray	30 μm	0.215−0.1 (25−300 ℃, 4 MPa, 1 m/s, 5 wt%); steel	1.75−0.5$\times 10^{-5}$ mm^3/(N·m)
	PTFE [136]	Steel	Electrostatic spray	30 μm	0.22 (25 ℃)−0.098 (180 ℃)−0.11 (300 ℃) (4 MPa, 1 m/s,7.5 wt%); steel	0.25−0.5$\times 10^{-7}$ mm^3/(N·m)

Matrix	Filler	Substrate	Methods	Thickness	Steady state friction coefficient	Wear rate/life
UHMWPE	Single wall carbon nanotube [166]	Steel	Dip coating	55 μm	0.08−0.16 (0−0.2 wt%) (4 N, 1,000 rpm) steel	6; 15; >25; >25×10^4 cycles
	Graphene [167]	Aluminum	Electrostatic spray	90 μm	0.33−0.30 (0 wt%−2 wt%) (2 MPa, 0.1 m/s); 0.32−0.20 (2−8 MPa, 0.1 m/s, 1 wt%); 0.27−0.14 (0.1−1.0 m/s, 4 MPa, 1 wt%) steel	37−18.2 (1.0 wt%); 18.2−56.1 (6 MPa); 40.6−50.9 μm/km
	C15A Organoclay [49]	Aluminum	Electrostatic spray	125 μm	0.16 (0 wt%); 0.18 (0.5 wt%); 0.17 (1.5 wt%); 0.15 (3 wt%)(9 N, 0.1 m/s) steel	5,000; 6,000; > 10,000; 8,500 cycles
	Carbon nanotube [50]	Aluminum	Dip coating	55 μm	0.1 (0 wt%)−0.016 (0.1 wt%) (45 N, 0.57 m/s) steel	25 (0 wt%)−200 (0.1 wt%)×10^4 cycles
	Carbon nanotube [129]	Silicon	Spin coating	5 μm	0.16−0.11 (1 wt%) (20 nN, 4 mm/s) steel	5−2×10^{-4} mm^3/(N·m)
	Graphite [28]	Steel	Dip coating	8−1.2 μm	0.074 (0 wt%)−0.061 (1 wt%) (0.5 N, 2.5 mm/s) steel	0.7−4×10^4 cycles
	Copper [168]	Steel	Dip coating	1.2 μm	0.07 (0.5 N, 2.5 mm/s) steel	20,000 cycles
PTFE	Epoxy [130]	Steel	—	100−150 μm	0.2−0.13 (50 wt%) (3 N, 0.025 m/s) steel	1×10^{-3} −3×10^{-6} mm^3/(N·m)
	Graphene oxide [127]	Stainless steel	Spin coating	—	0.15 (0 vol%)−0.05 (15 vol%) (5 N, 4 mm/s) 0.03 (15 vol%, 5 N, 4 mm/s,400 ℃) steel	26 (0 vol%)−2 (15 vol%) (400 ℃) ×10^{-7} mm^3/(N·m)
	Gold [29]	Stainless steel	Dip coating	0.2−0.5 μm	0.10 (0 wt%)−0.05 (0.06 wt%) (0.2 N, 2.5 mm/s); 0.09 (0 wt%)−0.07 (wt%) (0.5 N, 2.5 mm/s) chrome steel	307−608 cycles (0.2 N) 174−263 cycles (0.5 N)
	Polyparaben [128]	Bronze	Spray	15−20 μm	0.108 (0 wt%)−0.139 (20 wt%) (0.5 N, 0.1256 m/s) Gcr15 steel	13 (0 wt%)−3.9 (15 wt%) ×10^{-4} mm^3/(N·m)

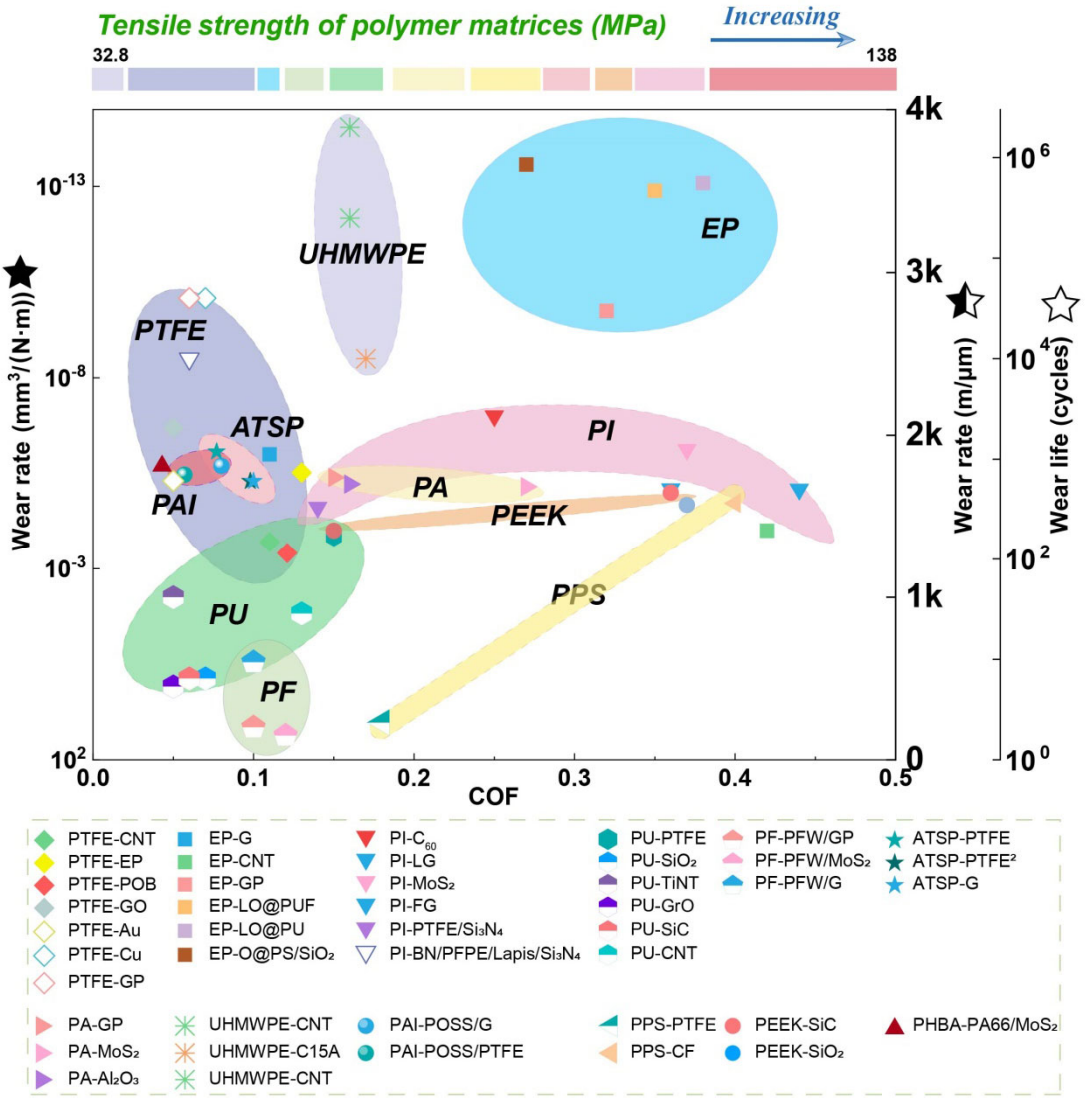

Fig. 4 Comparison of the tribological properties of different polymer matrices and different fillers.

a coherent transfer film. Further interaction between the bulk polymer and the transfer film gives rise to anisotropic deformation of the unit cell, resulting in the closeness of adjacent chains and easy shear between chains [126]. In summary, PTFE easily forms a uniform and strong transfer film on a metal surface, and its molecular structure leads to easy sliding. Therefore, the polytetrafluorethylene composite coating has a lower coefficient of friction than other polymers. Similarly, the friction coefficients of some PU and PAI coatings can also fall below 0.1. The friction coefficient of polyimide composite coatings containing different fillers varied from approximately 0.44 to 0.12, and the wear rates of these coatings are significantly different. The friction coefficient and wear rate of the composite coatings with the same matrix and different fillers are conveniently compared in Fig. 5.

Although PTFE has a low friction coefficient, its poor mechanical properties result in a high wear rate. Epoxy resin, carbon nanotubes, carbon fiber, graphene oxide, gold/copper nanoparticles, graphite, and other fillers have been added to enhance the tribological properties of PTFE composites, particularly the wear resistance. Nemati et al. [127] examined the effects of graphene oxide (GO) on the wear resistance of PTFE coatings. The micro- and macro-tribological test results indicate that the addition of GO effectively improves the wear resistance of the coating. When the PTFE composite coating contains

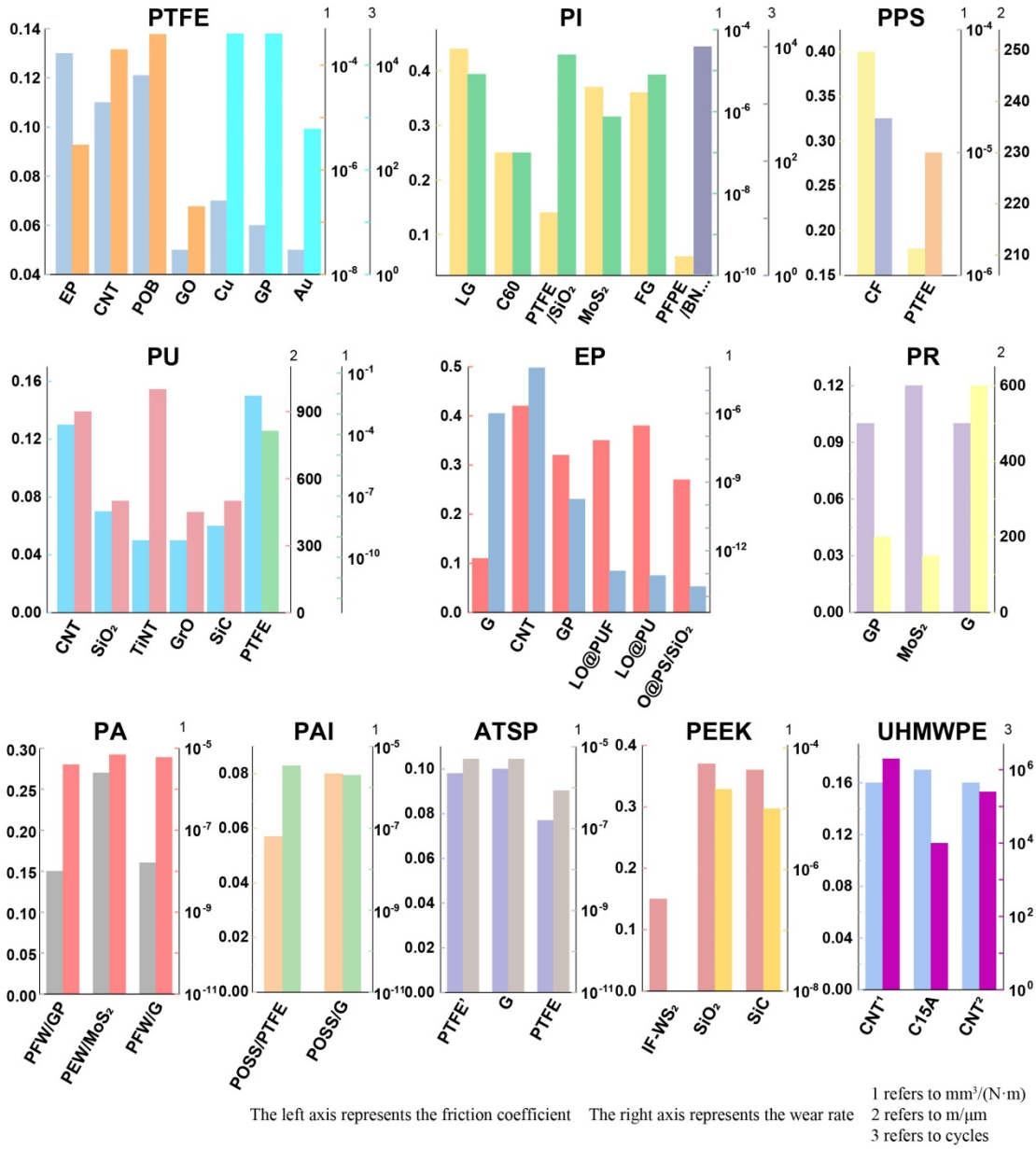

Fig. 5 Friction coefficient and wear rate of polymer composite coatings with different matrices.

15 vol% GO, the friction coefficient and wear rate is significantly reduced to 0.1 and 0.65×10^{-9} mm^3/(N·m), respectively. The wear rate of these composite coatings is two orders of magnitude lower than that of the pure PTFE coating. The homogeneous dispersion of high-strength GO in the low-friction PTFE matrix facilitates the formation of a self-lubricating film along the wear trajectory, as shown in Figs. 6(a) and 6(b). Likewise, adding 15 wt% polyparaben (POB) to PTFE can reduce the wear rate of the coating by 75%. The bearing capacity of POB reduces the shear and peeling of the PTFE matrix, which further reduces the adhesive wear caused by the transfer of PTFE to the grinding pair [128]. Carbon nanotubes [129] can also reduce the wear rate of the PTFE coating by 60%. Moreover, the addition of epoxy resin can reduce the wear rate of the PTFE coating by three orders of magnitude [130]. Graphite at 1.0 wt% in a PTFE coating can increase durability by five times and reduce the coefficient of friction by 17%. The aforementioned studies have emphasized the formation of a transfer film on the counterpart surface, which creates a low shear strength interface and exhibits exceptionally low friction and low wear rate [28]. In addition to

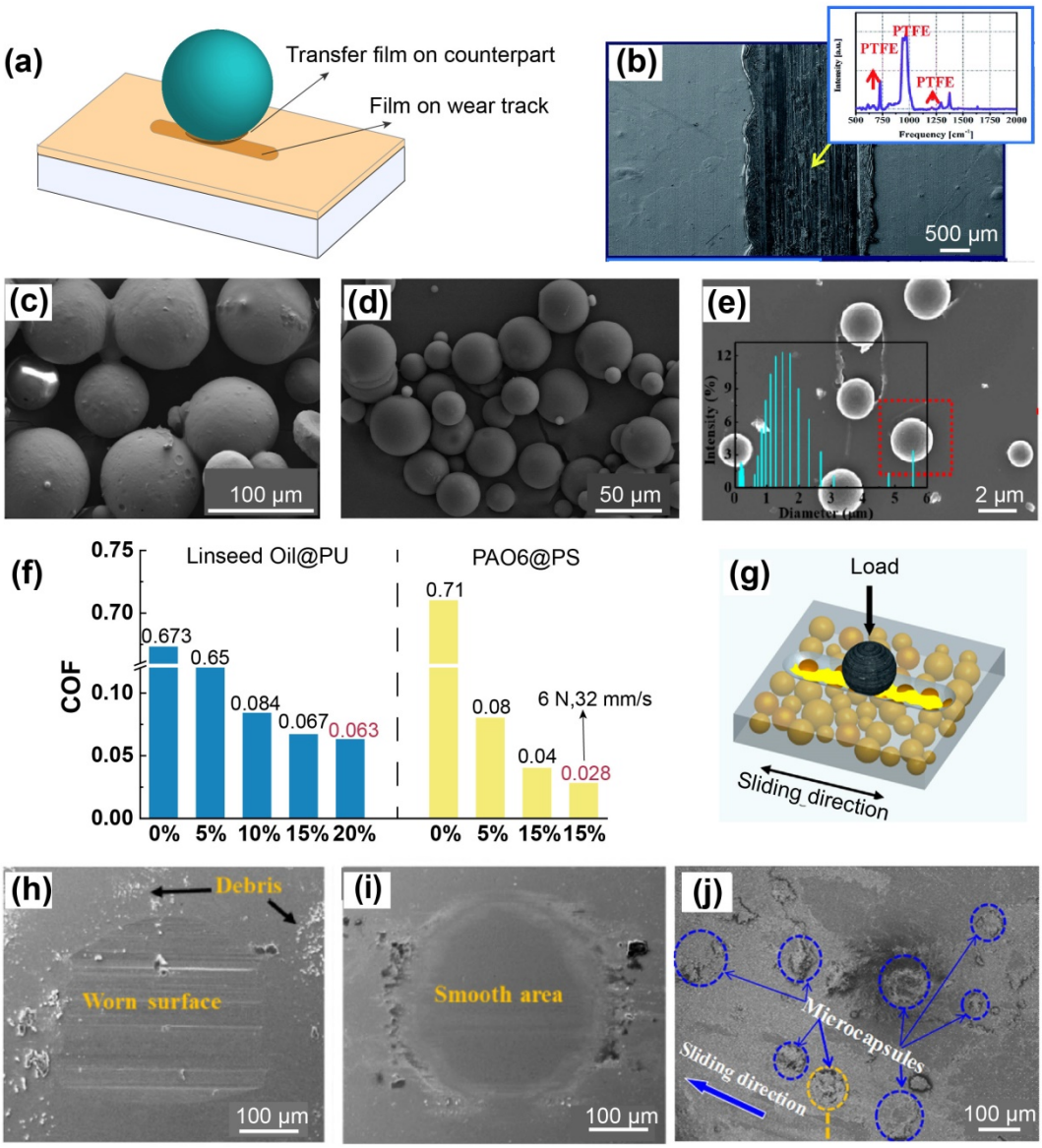

Fig. 6 (a) Schematic diagram of the lubrication mechanism of polymer composite coatings with solid fillers; (b) SEM images and Raman analyses of the wear tracks after 1,000 sliding cycles under 5 N normal load at ambient temperature of PTFE/GO coating. Reproduced with permission from Ref. [127], © Royal Society of Chemistry, 2016. SEM images of (c) tung oil@Polyureal microcapsules. Reproduced with permission from Ref. [92], © Elsevier B.V., 2017. (d) Linseed oil@polyurethane microcapsules. Reproduced with permission from Ref. [9], © MDPI, 2019. (e) PAO6@polystyrene microcapsule. Reproduced with permission from Ref. [10], © The authors, 2021. (f) Friction coefficient diagram of epoxy composite coating with different content of linseed oil@PU microcapsules (3 N, 5 cm/s) and PAO6@PS microcapsules (3 N, 16 mm/s and 6 N, 32 mm/s); (g) schematic diagram of the lubrication mechanism of oil-containing microcapsules. Reproduced with permission from Ref. [9], © MDPI, 2019. SEM images of the ball surfaces sliding against different composites: (h) pure EP resin, (i) composite with 5 wt% microcapsules. Reproduced with permission from Ref. [10], © The authors, 2021. (j) SEM images of the worn surface coating filled with 10 wt% tung oil-loaded microcapsules. Reproduced with permission from Ref. [92], © Elsevier B.V., 2017.

ordinary filler-type lubrication, surface modification of PTFE to enhance the wear resistance of PTFE coatings has been reported. Peng et al. [131] coated PTFE nanoparticles with polymethylmethacrylate (PMMA) by seed emulsion polymerization. The friction coefficient is 0.069 of the composite coating prepared by spin coating, and the wear volume is two orders of magnitude lower than that of the pure

PTFE coating. The presence of PMMA makes a continuous, uniform, and thin PTFE/PMMA composite film on its counterpart. Moreover, the existence of PMMA effectively improves the mechanical properties of PTFE.

PTFE is not only a coating matrix with excellent tribological performance, but also an effective lubricating filler for reducing the friction coefficient of other polymer coatings. As mentioned above, PI has excellent mechanical properties, but its friction coefficient is high. Su and Zhang [132] prepared PI composite coatings filled with PTFE and nano-Si_3N_4 by spraying technology and continuous curing. A PI composite coating with 20 wt% PTFE and 5 wt% modified nano-Si_3N_4 has the best tribological properties. Its wear rate is more than an order of magnitude lower than that of the unfilled PI coating, and its friction coefficient is more than two times smaller. After adding 40 wt% PTFE to the PPS coating, the friction coefficient was reduced from 0.36 to 0.17, and the wear life was increased to 250 m/μm [133]. The addition of modified oligomeric silsesquioxane (NH_2–POSS) significantly reduces the surface energy of the PAI/PTFE composite coating, thereby reducing the friction coefficient and wear rate. The NH_2–POSS/PAI/PTFE composite coating containing 7% NH_2–POSS exhibits the lowest friction coefficient and wear rate, respectively 0.07 and 3.4×10^{-6} $mm^3/(N\cdot m)$ [134].

The effects of PTFE on the tribological properties of a new material, ATSP, has also been investigated. The ATSP composite coating with 5 wt% PTFE achieves a low friction coefficient of 0.077 on dry friction and ultra-low wear rate of 8.50×10^{-7} $mm^3/(N\cdot m)$ [135]. In addition, Bashandeh et al. [136] measured the tribological properties of ATSP/PTFE coatings at high temperatures. The friction coefficient decreases with increasing temperature and is reduced by 54% at 180 °C compared with the friction coefficient at 25 °C. A substantial transfer film is formed on the counterpart during the friction process and increases with temperature, thereby providing a low wear rate and a stable coefficient of friction.

Other commonly used lubricating fillers include graphite, graphene, MoS_2, and PF/graphene composite coatings, and PAI/MoS_2 composite coatings have been reported. These fillers display excellent lubrication properties in the composite coatings owing to their layered structure with weak van der Waals interlayer interactions. Yu et al. [137] carried out an investigation of oligosilsesquioxane (POSS) modified PAI coatings with MoS_2 as filler, which demonstrated a low coefficient of friction and wear rates of 0.08 and 2×10^{-6} $mm^3/(N\cdot m)$. In addition to the lubrication effect of MoS_2, the cross-linking between the POSS and PAI also significantly contributes to the wear resistance of the composite coating. By admixing the PA coating with MoS_2 [138], the friction coefficient can be reduced to 0.15, and the wear rate can reach 10^{-5} $mm^3/(N\cdot m)$, which is 50% lower than that of a pure PA coating.

In addition to the above two-dimensional materials, black phosphorus (BP), with a layered structure, is a new kind of lubrication additive in water lubricants, oil lubricants [139], and solid lubricants [140]. The addition of BP nanosheets modified by NaOH (BP–OH) to water can result in robust superlubricity with a coefficient of friction of 0.006 [141]. Black phosphorus, with anisotropic frictional properties, acts as a lubricating filler based on its interlayer shear. When the micro-peaks move with each other, the ultra-thin BP nanosheets enter the contact area instead of being pushed away. When the contact pressure is applied to the micro-asperities in the contact area, they will not directly contact each other owing to the interlayer shear of the ultra-thin BP nanosheets [139, 141–143]. In addition, the remaining water layers on the surfaces of the BP–OH nanosheets also contribute greatly to the super-lubricity property [141, 143]. As a filler in the polymer coating, 5 wt% BP was added into the PTFE coating. The coefficient of friction of the PTFE/BP composite coating decreased to 0.046, with a 60% reduction from that of pure PTFE coatings, and the wear volume was reduced by 53% [144]. However, the degradation of BP with oxygen and moisture was considered an obstacle for its lubrication practices under ambient conditions. Wu Shuai found that the ambient degradation of BP significantly favors its lubrication behavior due to the combination of water molecules as well as the resulting chemical groups (P–OH bonds) formed on the oxidized surface [145].

Moreover, a super-slippery, degraded BP/SiO_2 interface was observed, and the interfacial liquid water was confirmed as a significant reason [146].

Several studies have confirmed the effectiveness of hard ceramic nanoparticles in improving the tribological properties of the coating, which is expected to enhance the adhesion of the transfer film to its counterpart [147]. Song and Zhang [70] found that the wear life increased from 1,250 to 2,750 m/μm for the PU composite coating with 3 wt% nano-silica and polytetrafluorowax (PFW), and the coefficient of friction slightly increased by 0.01. The addition of 5 wt% SiC nanoparticles and PFW into PU coatings reduced the friction coefficient and achieved a 100% increase in wear life [70], because the nanoparticle filler promoted the formation of a more uniform transfer film on the counterpart. This finding is consistent with the tribological test results of the PEEK/SiC composite coating. SiC nanoparticles significantly reduce the wear rate of the composite coating without excessive loss of coefficient of friction, especially under high loads. Under the test conditions of 9 N at 0.8 m/s, the wear rate of the PEEK/SiC composite coating is 1/3 that of pure PEEK. The role of SiC particles has been evaluated from two aspects. First, SiC particles may lead to energy dissipation by activating a fracture that occurs at the interface between PEEK and the powders. Second, it can effectively reduce the plows and adhesion between the two sliding parts [44].

All of the fillers mentioned above are solid fillers. Unlike liquid lubricants, they function without external supplements and subsequent maintenance. However, the lubrication effect of solid lubricants is far inferior to that of liquid lubricants. It is impractical to replace liquid lubrication with solid lubrication completely. In the short term, the best compromise is to combine solid and liquid lubricants. Previous studies have achieved effective lubrication by using porous solid materials that adsorb liquid lubricants as fillers. By mixing oleylamine into porous Cu–TBC metal–organic frameworks and forming an epoxy composite, ultralow friction (coefficient of friction ~0.03) was achieved [148].

Furthermore, microcapsule technology achieves the combination of solid lubrication and liquid lubrication, while solving the limitations of storage and replenishment of liquid lubricants. Microcapsules wrap the liquid lubricants in a solid shell through solvent evaporation or *in situ* polymerization. Li et al. [92] prepared tung oil microcapsules with a PUF shell through in-situ polymerization (Fig. 6(c)). A series of composite coatings were prepared with different contents of microcapsules, and tribological measurements were conducted. When the microcapsule content was 10 wt%, the friction coefficient (0.38) and the wear rate (8.26×10^{-14} mm^3/ (N·m)) was the lowest. Compared with the pure epoxy resin, the reduction was 17.3% and 78.6%, respectively. Apart from the lubricating effect of the oil film, the wear debris of the PUF shell was mixed with tung oil as a solid lubricant (Fig. 6(j)), enhancing the wear resistance of the epoxy coating. The PSF-coated tung oil microcapsules [92] prepared by the solvent evaporation method also effectively improved the tribological properties of the epoxy coating. Microcapsules with inorganic and organic materials as the collaborative shell layer can achieve outstanding tribological performance improvement. Containing 10 wt% microcapsules, whose shell is silica and polystyrene, the friction coefficient (0.27) of the epoxy coating is reduced by about 50% compared to the pure epoxy coating, and the wear rate (2.73×10^{-14} mm^3/(N·m)) is reduced by more than 80%.

The synergistic lubrication effect between SiO_2 nanoparticles in the shell and lubricating oil was proposed to explain the tribological behaviors. SiO_2 nanoparticles in lubricating oil decrease fuel consumption and effectively improve the wear resistance of lubricating oil. Moreover, SiO_2 nanoparticles can be filled into cracks caused by friction to prevent further wear of polymer composite coatings [95].

Although the addition of the above microcapsules improves the tribological performance of the epoxy coating, the friction coefficient of the composite coating is still approximately 0.2, equivalent to or even higher than that of conventional solid lubricants.

Yang et al. [9] encapsulated linseed oil with a polyurethane shell by interfacial polymerization (Fig. 6(d)) and mixed it with the epoxy coating. Figure 6(f) presents the friction coefficient of the epoxy composite coatings with different microcapsule contents. When the microcapsule content is 20 wt%, the friction coefficient of the composite coating decreases to a minimum of 0.06, which is reduced by 90.65% compared to that of a pure epoxy coating. In addition, Zhang et al. [10] prepared monodispersed polystyrene (PS)-encapsulated polyalphaolefin (PAO) microcapsules (Fig. 6(e)). The tribological properties of epoxy composites containing microcapsules under different loads and sliding speeds were studied. Compared with pure epoxy, the friction coefficient of composite materials can be reduced to 4% (from 0.71 to 0.028) (Fig. 6(f)), and the wear rate can be reduced by two orders of magnitude. The surface of the counterpart sliding against different composites is shown in Figs. 6(h)−6(i). The surface sliding against the composite is smoother, proving that the lubrication effect is related to the oil released from the microcapsules. These results fully demonstrate the advantages of microcapsules in terms of lubrication effects for achieving ultra-low friction coefficients in composite coatings.

The lubrication mechanism of the composite material containing microcapsules can be characterized by three processes. First, the microcapsules rupture due to pressure or shear during friction. The internal lubricant is released, and a boundary lubrication film is formed, which prevents the composite material from directly contacting the grinding pair, thereby reducing friction. (Fig. 6(g)) The release of lubricating oil has been confirmed by smooth wear surfaces and elemental analysis of the worn surfaces [9, 10, 92–94, 96, 149–151]. In addition, the cavity formed by broken microcapsules can be seen on the worn surface. Second, the cavity of the ruptured microcapsules can capture abrasive debris. The reduction in the amount of wear debris due to retention in the cavity weakens the abrasive effect of the wear debris as a third body in the contact area [92, 94, 149, 150]. Third, the cracked PUF shell can adhere to the film and the corresponding surface as a solid lubricant, which has a positive effect on reducing the friction coefficient and wear rate [93]. In addition, the nanoparticles in the shell layer can be used as additives for lubricating oil to reduce fuel consumption and effectively improve lubricity. In addition, nanoparticles can be filled into the cracks caused by friction to prevent further wear of the polymer composite coating [96].

Different fillers have unique advantages for improving the tribological properties of polymer coatings. In addition to the types of fillers, the content of the filler, the dispersion state of the filler, and the compatibility of the filler and matrix could also have a major impact on the tribological performance of the composite coatings. Moreover, the tribological performance is unambiguously associated with external factors such as the load, sliding speed, and temperature of the friction test [152, 153]. In a large number of studies on the tribological properties of composite coatings, the friction coefficient of coatings generally increases first and then decreases as the filler content increases, which indicates that there is an optimal value for the filler content. Too little filler is not sufficient to display its lubrication capacity. Similarly, too much filler is also not conducive to the increase in the friction properties of the coating because the properties of the composite coating deteriorate with the high filler content. The column of friction coefficient in Table 3 also describes the change in the friction coefficient with the filler content. For example, the friction coefficient and wear rate of epoxy/graphene composite coatings decreases with an increase in the graphene content from 0 to 4 wt% [154]. The friction coefficient of the epoxy/zinc sulfide-modified carbon nanotube composite coating [77] decreases first and then increases, reaching the lowest coefficient at 1.25 wt% (Figs. 7(a, b)). The mechanism reveals that when the content of a CNT/ZnS hybrid is less than 1.25 wt%, the fillers cannot be uniform, and they cannot effectively exert the lubricating effect. When its content exceeds 1.25 wt%, the fillers may easily agglomerate, which reduces the volume of the resin layer of the composite materials and weakens the bonding force between the epoxy resin and the filler. The wear life of the PPS/PTFE composite coating [133] is

significantly reduced when the volume fraction of PTFE is too low or too high (Fig. 7(c)). PTFE particles will agglomerate in the coating when the volume concentration is low. However, when the volume concentration is high, the adhesive is insufficient to bind each PTFE particle, and the coating is easily deformed and smeared, resulting in severe wear of the coating.

Furthermore, both the dispersion of the filler and the compatibility of the filler and the matrix also affect the tribological performance of the coating. Generally, surface modification is utilized to improve the filler dispersion and compatibility with the matrix, further elevating the lubrication effect of the filler. For example, Li et al. [77] overcame the problem of poor dispersion of CNTs in the polymer matrix by the in situ synthesis of zinc sulfide (ZnS) nanoparticles on the CNT surface (Fig. 7(d)). As a result, the composite coating containing CNT/ZnS exhibited better tribological performance than the composite coating containing untreated CNTs. In order to improve the dispersibility and compatibility of fullerenes in epoxy, Liu et al. [74] treated fullerenes with the silane coupling agent

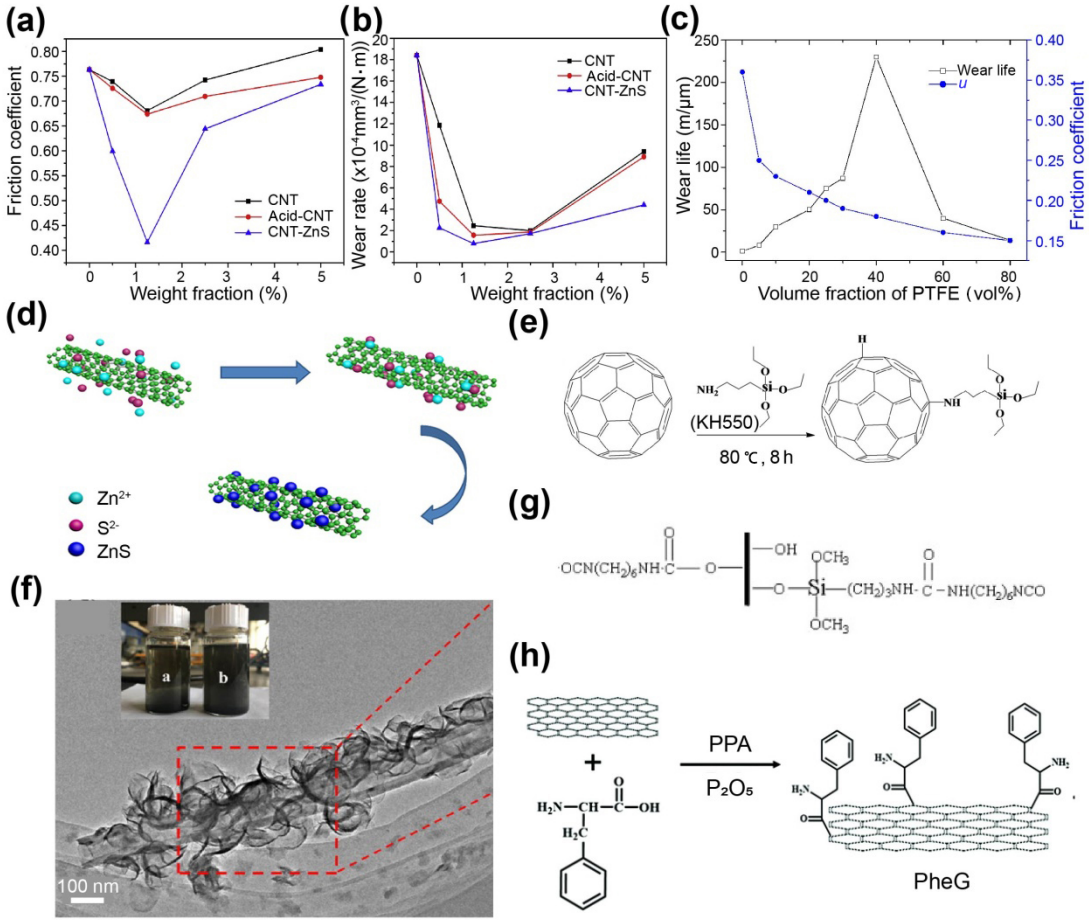

Fig. 7 (a) Friction coefficient and (b) wear rate of EP, EP–CNTs, EP–acid–CNTs, and EP–CNTs/ZnS coatings. Reproduced with permission from Ref. [77], © Elsevier, 2018. (c) Effect of volume concentration of PTFE on the friction and wear behaviors of the polyphenylene sulfide coatings (1.25 m/s, 320 N, 40 μm). Reproduced with permission from Ref. [133], © Elsevier, 2009. (d) Schematic illustration of synthesis of CNTs/ZnS hybrid. Reproduced with permission from Ref. [77], © Elsevier, 2018. (e) Reaction scheme between fullerene and KH550. Reproduced with permission from Ref. [74], © Elsevier, 2016. (f) TEM images of MoS_2@HCNF hybrid with 20 mg of HCNF (the insets are the optical photos of MoS_2-PAA/DMAC-a and MoS_2@HCNF–PAA/DMAC-b stationary dispersions). Reproduced with permission from Ref. [5], © Elsevier B.V., 2017. (g) Schematic diagram of HDI modified TiO_2 nanotubes. Reproduced with permission from Ref. [155], © Elsevier B.V., 2008. (h) Schematic diagram for the modification of graphene. Reproduced with permission from Ref. [25], © Royal Society of Chemistry, 2019.

3-aminopropyltriethoxysine (KH550) (Fig. 7(e)). Several studies have used hexamethylene diisocyanate (HDI) to modify titanium dioxide nanotubes (Fig. 7(g)) [155] and toluene-2, 4-diisocyanate (TDI) to modify carbon nanotubes [156] to improve the bonding and compatibility of fillers in the PU coatings. Moreover, MoS_2 was grafted onto the surface of CNTs (Fig. 7(f)) to promote its dispersibility in the PI coatings [5]. Graphene nanosheet edges were aminated with L-phenylalanine (PheG) (Fig. 7(h)) to realize good dispersion of graphene in PI coatings [25].

4 Mechanical properties of polymer composites coatings

The mechanical properties of polymers are mainly characterized by three essential indices: stiffness (elastic modulus), strength (tensile strength), and toughness (elongation at break). These properties play a critical role in the service quality and service life of the coatings. Outstanding mechanical properties enable the coating to adapt to more severe working conditions and increase the service life of the coating. Although some polymers have an excellent tensile strength and Young's modulus, they still lack some critical characteristics, such as impact strength or toughness. Further improvement of the mechanical properties of polymer coatings remains a major challenge. The mechanical properties of polymer coatings are generally enhanced by adding fillers with excellent mechanical properties, such as graphene, carbon nanotubes, and ceramic nanoparticles, called reinforcing phases in polymer composite coatings. Based on the morphology, reinforcing fillers are divided into 2D fillers, 1D fillers, and 0D fillers, as shown in Fig. 8. 2D reinforcing fillers mainly include graphene and nanoclays. Carbon nanotubes and fibers (carbon fiber and glass fiber) are common 1D fillers. 0D reinforcing fillers are mainly ceramic nanoparticles, including silica, alumina, and silicon nitride, and many more. Spatial orientation, content, size,

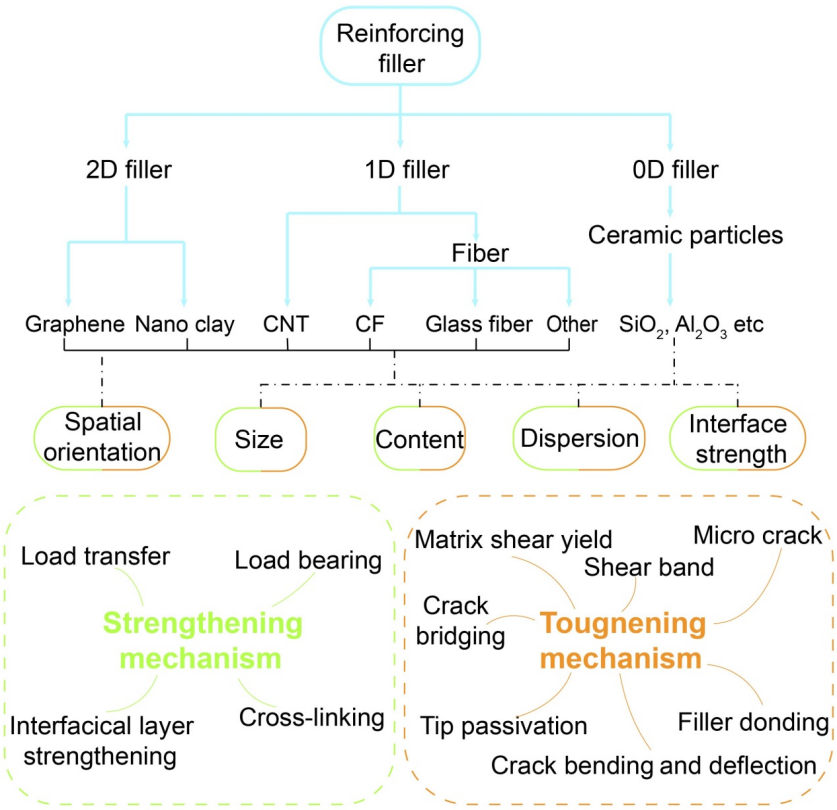

Fig. 8 Classification of reinforcing fillers, influencing factors of reinforcement effect, and strengthening and toughening mechanism.

dispersibility, and interfacial strength are the principal factors determining the reinforcing effect of the fillers. Fully understanding the strengthening and toughening mechanism can maximize the mechanical properties by optimizing the size, spatial orientation, and content of fillers. In the following paragraphs, the strengthening and toughening mechanisms of these three types of fillers are summarized and introduced in Fig. 8. A schematic diagram of the strengthening and toughening mechanisms is shown in Fig. 9.

To date, the strengthening mechanism of 0D reinforcement in rubbery and molten polymers has been analyzed sufficiently, including particle jamming, strain field distortion [169], polymer fixation, and dynamic changes between tightly packed particles [170], and polymer bridges between nanoparticles [171, 172]. A strong relationship has been established between the enhancement of rubbery and molten polymers and the aggregation state of the reinforcing particles. The working temperature of polymers used in coatings is usually lower than the glass transition temperature, and thus the polymer is in a glassy state, and the reinforcing nanoparticles in the glassy polymer are naturally uniformly distributed. Thus, there is a certain deviation in the applicability of the above theory. The following discussion seeks to review the mechanical properties and mechanisms suitable for glassy polymers.

Enhancing the stiffness and strength of polymer composites can be described by classical composite theory. Stress transfer between the matrix and filler and the load bearing of fillers are the main mechanisms. When the composite is subjected to external stress, the matrix stress is transferred to the fillers through the matrix-filler interface, and fillers become the main load-bearing phase. The elastic modulus and tensile strength of the filler are higher than those of the matrix, so the polymer material is reinforced [173]. Chih et al. [174] examined the strengthening effect of graphene nanosheets, 2D fillers, on ultra-high molecular weight polyethylene coatings. For composite coatings containing 2–5 wt% graphene, the modulus of elasticity increased by 10%. However, the actual reinforcement effect is decidedly inferior to the expected reinforcement effect, due to particle agglomeration leading to a decline in the

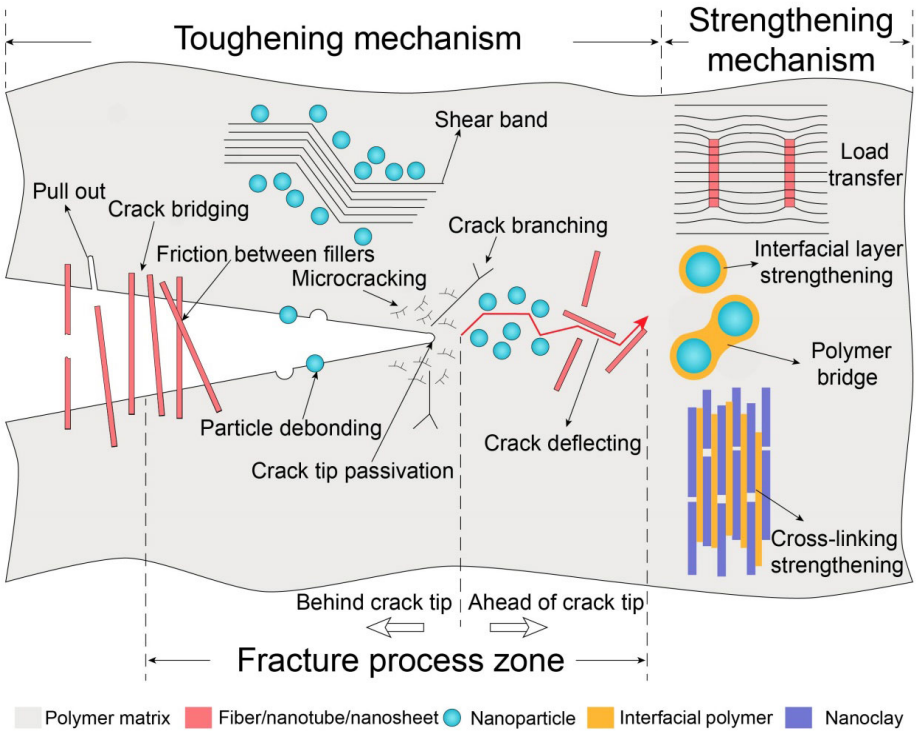

Fig. 9 Schematic diagram of strengthening and toughening mechanism of polymer matrix.

stress transfer. Samad and Sinha [166] added 0.2 wt% carbon nanotubes, 1D fillers, to a UHMWPE coating, increasing the hardness of the coating by 66% and the elastic modulus by 58%.

The stress transfer mechanism is applicable to all three types of reinforcing fillers, and the size, content, and dispersion state of the fillers also have a significant impact on the reinforcing effect [175]. In a study of particle size effects on the strength of PA 6/silica nanocomposites, the average particle sizes added were 12, 25, and 50 nm. The particle additions increase strength, and smaller particles provide better reinforcement [176]. Maillard et al. [177] carried out a series of tests on the mechanical

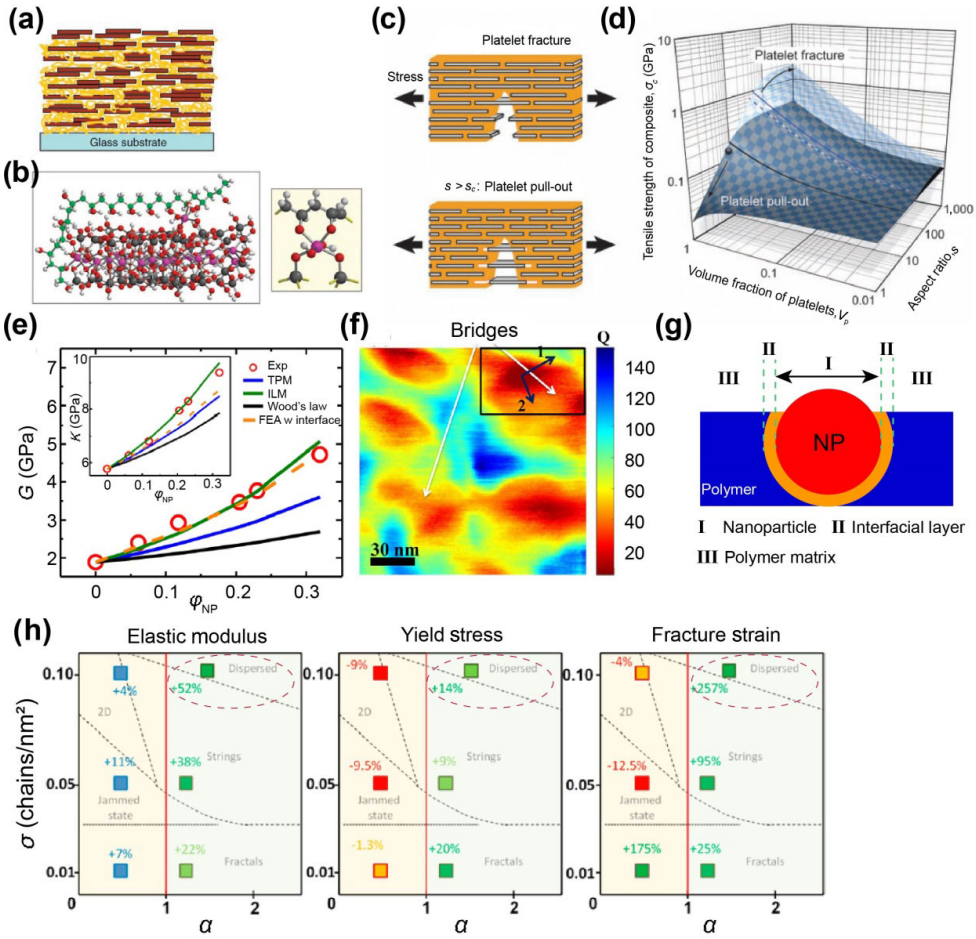

Fig. 10 (a) Schematic representation of the internal architecture of the PVA/MTM nanocomposite (picture shows 8 bilayers). Reproduced with permission from Ref. [64], © American Association for the Advancement of Science, 2007. (b) Energy-optimized geometry of bonding between PVA and MTM via Al substitution sites obtained by computer calculations with the AM1 semi-empirical algorithm. (Right) Enlarged portion of the six-membered cycle formed between PVA and MTM. Al, purple; O, red; H, light gray; Si, dark gray; C, green. Reproduced with permission from Ref. [64], © American Association for the Advancement of Science, 2007. (c) Fracture mechanisms and (d) estimated tensile strength of platelet-reinforced composites. Reproduced with permission from Ref. [179], © American Association for the Advancement of Science, 2008. (e) Shear modulus, *G*, and bulk modulus (inset), K, for PNCs with different loadings estimated from the BLS data. The lines are fits to continuum mechanics based on Woods' law, a two-phase model (TPM), an interfacial layer model (ILM), and the dashed-orange lines are predictions by a simulation of finite element analysis (FEA) with an interfacial layer. Reproduced with permission from Ref. [182], © American Chemistry Society, 2016. (f) Q-factor (the bandwidth of the resonance peak) of the cantilever map of the surface. Reproduced with permission from Ref. [182], © American Chemistry Society, 2016. (g) Schematic representation of nanoparticles in a polymer matrix and three regions of the composite. Reproduced with permission from Ref. [182], © American Chemistry Society, 2016. (h) Reinforcement percentage of the elastic modulus, yield stress, and failure strain relative to the pure polymer depending on grafting density and grafted/ matrix chain length ratio. The loading of the silica core was 5 mass % in all the samples. Reproduced with permission from Ref. [177], © American Chemistry Society, 2012.

properties of polystyrene films reinforced with grafted silica in different dispersion states. The results demonstrated that well-dispersed silica could simultaneously improve the elastic modulus, tensile strength, and toughness. However, aggregated silica nanoparticles led to varying degrees of reduction in tensile strength and toughness (Fig. 10(h)). Moreover, both the elastic modulus and tensile strength increased with increasing silica content.

In addition to the filler content, the size of the fillers also plays a vital role in strengthening. A large number of experimental studies on fiber-reinforced composite materials show that short fibers have an inferior reinforcing effect on polymer composites compared with longer or continuous fibers. This phenomenon has been explained in detail through shear lag and other theories. Only when the fiber is longer than the critical length can excellent mechanical properties be obtained. The main parameters affecting the critical length are the aspect ratio of the nanosheets and the interfacial interaction between the filler and the matrix. In addition, for 2D fillers and 1D fillers, the spatial orientation of the fillers will also significantly affect the reinforcing effect [173, 178]. Mortazavian and Fatemi [178] confirmed that the tensile strength of the composite changes nonlinearly with the angle of orientation in a given plane of the glass fiber in the sample.

In addition to the stress transfer mechanism, the interaction between the matrix and the filler can also increase the strength of the polymer material. Covalent bonding, hydrogen bonding, and physical entanglement between the nanoclay and polymer increase the strength of the polymer in the nanoclay gap and facilitates the interfacial stress transfer (Fig. 10(a)). Podsiadlo et al. [64] proved the covalent connection between poly(vinyl alcohol) (PVA) and montmorillonite through theoretical simulations (Fig. 10(b)) and experimental measurements, which led to the effective hardening of the matrix and improved the tensile strength by a factor of 10 compared to that of pure PVA. Bonderer et al. [179] used alumina flakes to increase the tensile strength of the chitosan matrix by 6 times. Chan et al. [180] prepared uniformly dispersed nanoclay/epoxy composite samples, and Young's modulus and tensile strength of the composites containing 5 wt% nanoclay increased by 34% and 25%, respectively. In the same study, scanning electron microscopy (SEM) and transmission electron microscopy (TEM) analysis confirmed the interlocking and bridging effect between nanoclay and matrix in the composite material. This result is explained by the fact that nanoclay clusters enhance the mechanical interlocking inside the composite, thereby destroying crack propagation. A composite of nylon 6 and nanoclay also achieved a 200% increase in Young's modulus and a 175% increase in tensile strength [181]. The addition of nanoparticles to a glassy polymer results in a higher strength between the polymer and the nanoparticles than the strength of the matrix (Fig. 10(g)). Cheng Shiwang et al. [182] directly observed a 2–3 nm interfacial layer in a PVA/SiO_2 composite through the combination of small-angle X-ray scattering (SAXS), Brillouin light scattering (BLS), and atomic force microscopy (AFM) measurements, providing experimental evidence of polymer bridges between nanoparticles in polymer nanocomposites (Figs. 10(f) and 10(g)). In this study, Young's modulus of the interfacial polymer layer is two times higher than that of the matrix polymer, indicating that nanoparticles significantly enhance Young's modulus in PVA below the T_g (Fig. 10(e)). The article also states that the results should be applicable to various types of glassy polymer nanocomposites.

Based on the above analysis, the reinforcing properties of a polymer composite are directly related to the interfacial bonding strength between the polymer matrix and the filler. Good interfacial bonding properties help to transfer stress while suppressing the generation of cracks, which in turn enhances the mechanical strength. Weak interfacial bonding will cause problems such as stress concentration at the filler interface and reduce the mechanical properties of the polymer material. Surface modification, including physical adsorption or chemical grafting of fillers, was performed to improve the binding between fillers and the polymer matrix. Furthermore, it is necessary to avoid the aggregation of fillers. Achieving a good dispersion is also an effective way to enhance the mechanical properties of polymers.

The strengthening effects of the three reinforcing fillers are different owing to their large variations in spatial morphology. The 2D fillers are lamellar and have a large aspect ratio, and the in-plane size is much larger than the longitudinal thickness. 1D fillers also have a large aspect ratio. 0D fillers are generally spherical, and the aspect ratio is minimal. Okumura et al. [183] investigated the mechanical properties of PA6/hydroxyapatite composites, and the shape of the fillers in the composites was controlled to 0D (particle), 1D (needle), and 2D (plate). The results indicate that each nanofiller (0D, 1D, and 2D) exhibits different effects. 0D fillers are known to enhance the mechanical properties and are generally easier to synthesize than 1D or 2D fillers. Owing to the high aspect ratio (L/d), 1D fillers can enhance the mechanical properties, especially the tensile strength, more effectively. On the other hand, 2D fillers have been shown to improve the barrier effect and mechanical properties, especially the bending characteristics. Scotti et al. [184] also studied the effect of particle morphology on the filler reinforcing effect. Compared with spherical particles, anisotropic rod-shaped particles can provide stronger reinforcement to rubber, and by increasing the aspect ratio of the particles, the effect will be enhanced. Many researchers have investigated the reinforcing ability of 1D, 2D, and 3D fillers, which concluding that the reinforcement effect of a 1D filler is better than that of a 2D material, and the reinforcing effects of 1D and 2D materials are greater than those of the 3D filler [185−187]. Nadiv et al. [186] introduced a robustness factor to measure the filler concentration range necessary for achieving a significant reinforcing effect, and the robustness factor increased with filler dimensionality. In fact, any deviation in the concentration of 2D or 3D fillers did not dramatically change the nanocomposite performance. Considering robustness and reinforcing efficiency, 1D and 2D materials constitute attractive fillers. The better reinforcing effects of the 1D and 2D fillers may be related to the larger filler/polymer interfacial area caused by the high aspect ratio [173, 183, 184, 186].

Toughness is another critical property of polymer materials. Unilaterally increasing the strength of the polymer and sacrificing its toughness weakens the defect resistance of the polymer, which is not conducive for its use in polymer coatings. Toughness has a strong correlation with crack growth. Increasing the path of crack growth, reducing the speed of crack growth, and increasing energy dissipation are effective approaches to toughening the composite. Proposed toughening mechanisms of polymer materials discussed in literature reviews of this research mainly include crack bridging and filler extraction, shear yield of the diffusion matrix, the formation of shear bands, microcracking, crack pinning, crack tip passivation, crack deflection, and interfacial debonding of the filler matrix [175].

The toughening mechanism varies with different fillers. The main toughening mechanism of nanoclays, carbon nanotubes, or carbon fibers is crack bridging and pulling out. When cracks propagate, certain fibers hinder their expansion. With increasing applied energy, cracks grow around the fiber, which is called crack bridging. This mechanism works until the matrix around the fiber breaks completely, and the fiber loses its reinforcing effect, after which the fiber is pulled out from the matrix by the continued applied force. The size of the nanoclay and fibers is also a critical factor in the toughening process. When the size is smaller than the critical size, the matrix material will fail around the filler, and the filler is pulled out. However, when the size is greater than the critical size, the stress will be completely transferred to the filler, and the filler is more likely to be broken, eliminating the toughening effect [179, 188, 189]. Bonderer et al. [179] pointed out that there is a critical value for the aspect ratio of nanoclays. For platelets with an aspect ratio above the critical value, the composite material will fail because of fracture of planets, resulting in brittle fracture. For platelets with an aspect ratio below the critical value, the continuous matrix yields before the platelets rupture, resulting in a toughening behavior. For example, a possible scenario involves the platelets pulling out and the matrix plastically flowing before the composite is completely ruptured (Figs. 10(c) and 10(d)).

The toughening mechanisms of 0D fillers are different from those of 2D fillers and 1D fillers

owing to their small aspect ratio. The energy dissipation associated with the displacement of the fillers and the formation of shear bands is confirmed as the dominant toughening mechanism of 0D fillers. Because of the strong interfacial interaction between the nanoparticles and the matrix, crack nucleation is suppressed and the shear bands nucleate in the polymer matrix. As the dispersibility of the particles increases, the propagation paths of these shear bands increase, resulting in increased toughness of the matrix [177, 188]. The other primary mechanism is crack bending (crack pinning). In the presence of hard particles, the crack will be immobilized, and the propagation is locally interrupted. If it continues to proceed, it needs to bend around the particle, which requires more energy. The crack deflection mechanism is the same. However, when the binding force between the particles and the matrix is weak, the particles and the matrix will separate, called particle debonding. Crack tip passivation is also an important mechanism of particle toughening.

The improvement of the mechanical properties of polymer composite coatings can increase the load-bearing capacity of coatings. Perfluoroalkoxy (PFA) coatings filled with Al_2O_3 exhibit a higher load-bearing capacity under sliding conditions [190]. PA6/CNT composites have a higher load-bearing capacity than pure PA6. Higher tensile strength and Young's modulus also result in a higher load-bearing capacity of the composite [69]. The improvement in the bearing capacity of the composite material means that it is not easy for the material to undergo plastic deformation during friction with the grinding pair, and it does not easily to peel off and fall off. At the same time, it can maintain the structural integrity of the composite material under a high load [191]. Therefore, the wear resistance is enhanced. In addition, excellent mechanical properties can significantly inhibit the generation and propagation of cracks on the worn surface, thereby improving wear resistance [192]. Surface hardness is one of the most critical factors that determines the wear resistance of a material. Harder surfaces have a higher wear resistance. The improved wear resistance observed in the SiO_2/short carbon fiber/epoxy hybrid composites is due to the improvement in the surface hardness [68]. In short, the enhancement of polymer mechanical properties can improve its friction performance to a certain extent.

5 Adhesion properties of polymer composites coatings

Good adhesion of the coatings to the substrate is fundamentally necessary for excellent frictional and mechanical properties of the coating because the integrity of the coating is dependent on the integrity of the interface. Various internal or external forces, including mechanical stress, thermal stress from the environment, and corrosion, will cause the coating to fail to adhere. Testing of the adhesion of a coating to a substrate is of particular significance. Adhesive strength measurements can provide guidance for the design and selection of better coating application methods and good coating–substrate systems. To date, widely used coating adhesion tests include micro- and nanoindentation, micro- and nano-scratch, blister, bump, bend test, and pulsed laser-induced impact spalling. Many different measurements, detection methods, and characterization techniques are associated with these local damage tests, including acoustic emission detection, thermal and infrared thermal imaging, laser interferometry, raster scanning microscopy techniques such as atomic force microscopy, acoustic probe microscopy, scanning electron microscopy, scanning electrochemistry microscopy, and Raman spectroscopy.

Micro- and nanoindentation tests not only measure coating hardness, Young's modulus, and other properties through continuously recorded force and indentation depth, but also perform quantitative, semi-quantitative, and qualitative tests on coating adhesion. Good adhesion at the interface is shown as a smooth transition from the coating to the substrate (or primer) on the indentation profile, while poor adhesion will show an uneven transition. Depending on the position of the indenter, the indentation test can be an interfacial indentation, a surface indentation, or

cross-sectional indentation (Figs. 11(a) and 11(b)). The scratch test [193] applies an increasing force using an indenter as the sample is moved tangentially. The force sensor measures both vertical force and friction, and can also record the indentation depth and lateral displacement. Finally, the generated stress will cause the coating on the substrate to chip, peel, or crack, as shown in Fig. 11(c). The minimum friction force that causes the coating to fail is the critical force. In addition, lasers can also be employed to cause coating failure. The blistering, bulging, and bending tests are suitable for checking the interfacial adhesion of elastic or flexible coatings to plastic or rigid substrate systems. For the blister test, an external force (or pressure) is applied to the back surface of the test coatings through the entrance hole and then causes blistering, swelling, and bending phenomena, as shown in Fig. 11(d). Depending on the external force method, the test may result in a shaft-load blister, a thermally-induced blister, or a hydraulic/pneumatic blister. Pulsed laser-induced impact spallation can test the dynamic failure of the coating due to delamination, also known as laser spallation. The laser pulse hits the absorption layer, producing a strong, high-amplitude acoustic pulse wave, which propagates through the thickness of the substrate to the test coating and reflects on the free surface of the coating. This will cause interference of incident light and reflected waves, which will affect the interfacial stress. Delamination and flaking may occur when the stress reaches the critical interfacial strength of the coating. In addition, Table 4 summarizes the applicability of indentation, scratching, blistering, and laser peeling tests in different coating–

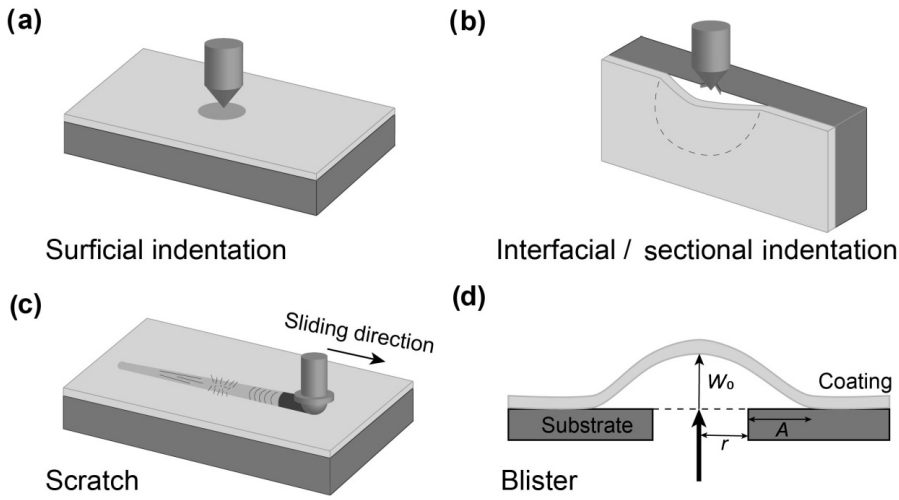

Fig. 11 Schematic diagram of partial test method for coating adhesion. (a) Surficial indentation; (b) interfacial/sectional indentation; (c) scratch test; and (d) lisbter test.

Table 4 Suitability of different test methods for coating-substrate systems.

	Thin coating (<20 μm)				High coating (>20 μm)			
	D-B	D-D	B-B	B-D	D-B	D-D	B-B	B-D
Interface indentation	✓	—	✓	✓	—	—	—	—
Surface indentation	—	—	—	—	✓	—	✓	✓
Cross-section indentation	—	—	—	—	✓	—	✓	✓
Scratch (by load)	✓	—	✓	✓	—	—	—	—
Scratch (by laser)	—	—	—	—	✓		✓	✓
Blister	✓	✓	—	—	✓	✓	✓	—
Laser spallation	✓	✓	—	—	✓	✓	—	—

Note: D-B means coating-substrate systems. B means brittle and D means ductile.

substrate systems [194]. In addition to the above methods, the solvent immersion test and the tape test are also utilized to evaluate the adhesion properties. Moreover, Hopkins et al. [195] proposed a combination of calculations and peeling experiments to determine the interfacial characteristics of polyurethane stent coatings bonded to stainless steel. The delamination of the stent coating under dry and hydrated conditions was studied in 90 peel tests, and the measured force and peel radius were used to determine the interfacial properties. There are also studies using ultrasound to evaluate the adhesion properties of coatings [196].

A large and growing body of literature has been devoted to improving the adhesion between coatings and substrates to enhance coating performance. Current enhancement methods mainly focus on treating the surface of the substrate and using a suitable adhesive. The surface treatment of the substrate can either be mechanical, chemical, and/or energy treatments. Mechanical processing mainly includes mechanical polishing, shot blasting, acid etching, laser processing, and anodizing etching, which increase the macro or micro roughness, further increasing the area and strength of the interaction between the coating and the substrate. Theoretical simulations by van Tijum et al. [197] showed that local delamination competes with roughening at the interface, which eventually leads to an increase in the adhered area. van den Brand et al. [198] immersed an aluminum substrate in boiling water to hydrate aluminum, forming a pseudoboehmite layer with a porous structure, into which the epoxy coating completely penetrated (Figs. 12(a) and 12(b)). High hydroxyl density, large surface area, and porosity resulted in outstanding adhesion properties of the system. van Dam et al. [199] studied the effect of surface roughness on the adhesion of epoxy coatings. The initial adhesion is enhanced with the increase in the surface roughness due to the increase of the interfacial bonding area under higher surface roughness. However, the improvement in the durability of the coating is not obvious because these techniques mainly rely on inducing mechanical interlocking and van der Waals forces, which are very susceptible to high temperature and humidity conditions. Shot blasting and acid etching were employed to produce the porous surface morphology, triggering possible mechanical interlocking. The

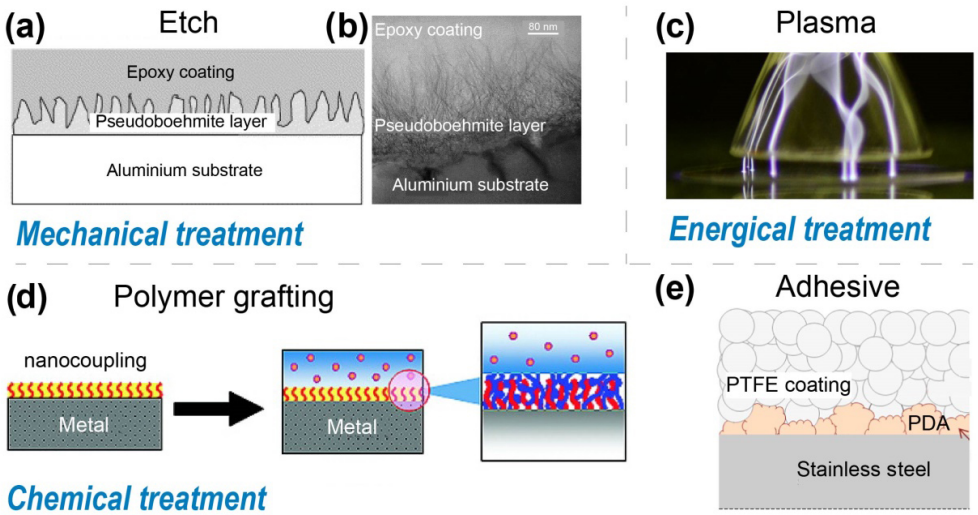

Fig. 12 Methods for enhancement of coating and substrate adhesion. (a) Hydration of the aluminum substrate by immersion in boiling water, resulting in the formation of a porous pseudoboehmite oxyhydroxide layer. The epoxy coating fully penetrates into this porous structure; (b) TEM cross-section image of the epoxy–pseudoboehmite–aluminum system. Reproduced with permission from Ref. [198], © Elsevier B.V., 2004. (c) Image of atmospheric pressure plasma jet. Reproduced with permission from Ref. [209], © Taylor & Francis, 2004. (d) Schematic illustrations of the preparation of nanocoupling process, Reproduced with permission from Ref. [202], © American Chemistry Society, 2011. (e) Schematic diagram of coating with PDA as adhesive. Reproduced with permission from Ref. [28], © Springer Verlag, 2016.

adhesive penetrates the surface pores to form the so-called micro-composite interphase region. Therefore, the presence of complex textures or morphologies has a greater impact on the initial adhesion and persistence of interfacial adhesion than the average roughness. Krzywiński and Sadowski [200] also improved the adhesion between the epoxy resin and concrete substrates by preparing surface textures, including slotting, embossing, gripping, and brushing.

Chemical treatment mainly involves cleaning the substrate with organic solvents, chemically grafting the polymer on the surface, and applying primer/adhesive to form a sandwich structure of the substrate, adhesive layer, and coating. Jaeho et al. [201] reported an effective method for increasing adhesion by grafting an organic layer to a steel surface. Because the interaction between the molecular chain of the polymer coating and the organic layer covalently grafts to the metal surface, the adhesion between the polymer and the steel surface is improved by more than 100%. Choi et al. [202] introduced oligolactic acid onto the surface of stainless steel, and the thickness of the oligolactic acid graft was maintained at the nanometer level. The nanocoupled stainless steel sample exhibited the most durable interfacial adhesion between the polymer coating and the metal substrate (Fig. 12(d)). Grafting of polycaprolactone and ricinoleic acid on a substrate surface enhances the adhesion between the polymer coating and the substrate. A thin polymer interfacial layer is applied between aluminum and epoxy resin, which participates in the curing of the epoxy coating [203]. Systems based on poly (ethylene-alt-maleic anhydride) show good adhesion strength and durability due to the formation of cured and mixed epoxy/polymer interphase regions [198]. A self-assembled monolayer film of 3-aminopropyltrimethoxysilane (APS) was formed on an aluminum substrate by covalent bonding. The APS single-layer film acts as a covalent bond between the polymer coating and the aluminum alloy substrate, enhancing the adhesion properties of the polymer coating [204]. In addition, the coating material can also be grafted to enhance the adhesion behavior. Polypropylene with 3 wt% maleic anhydride (MAH) can provide high values for adhesion strength, Young's modulus, and breaking strain [205]. By introducing a silane reagent (3-aminopropyl triethoxysilane) that can covalently bond with PU on a tin surface, the adhesion of PU can be increased [206].

A silane coating can also be utilized to enhance the adhesion between PPS and stainless steel [207]. Although the silane coating does not change the morphology of the substrate, the chemically modified surface has proven to be more resistant to delamination [199]. Polydopamine (PDA) is used as an adhesive to enhance the adhesion of the PTFE coating to the substrate (Fig. 12(e)). The linearly increasing load scratch test shows that the increase in durability is also the result of the improved adhesion between the PTFE topcoat and the PDA primer. The use of PDA also prevents large-scale delamination of the coating [28].

Options for energy treatments mainly include plasma treatment, ultraviolet irradiation, and ozone radiation. Oxygen plasma treatment of a substrate (Fig. 12(c)) can improve the adhesion of PU on the PU substrate surface [208, 209]. Plasma exposure does not cause significant changes in morphology or surface roughness. The central role of plasma is surface activation and cleaning. In addition, studies have shown that thermally assisted plasma treatment of PTFE [210, 211] can promote the formation of carbon-carbon crosslinks on the surface of PTFE and the etching of weak boundary layers, which greatly improves the adhesion strength of PTFE. Hamdi et al. [212] found that when primer coating and UV/ozone radiation were applied, the adhesion of acrylonitrile butadiene styrene increased.

6 Summary and outlook

This review provides a survey of the properties of conventional polymer coating matrices, types of fillers, and preparation methods of coatings. It also summarizes the tribological properties of different polymer composite coatings. The addition of solid fillers can promote the formation of polymer transfer films. Microcapsules also contribute to forming a liquid lubrication film, which significantly reduces

the friction coefficient of the pure polymer matrix or improves the wear resistance. The addition of reinforcing fillers enhances the strength of the coatings by effective stress transfer and the enhancement of the polymer interfacial layer, and improves the toughness of the coating by crack bridging and filler extraction, shear yielding, and crack deflection. Reasonable substrate treatment methods, such as mechanical treatment, chemical treatment, and energy treatment, can improve the adhesion between the coating and substrate. It is worth pointing out that this article only briefly discusses the influence of external environments such as load, velocity, and temperature on coating performance, but these are still key factors affecting the coating performance.

The choice of a polymer matrix for a composite is based on the preset operating conditions and the desired temperature resistance and mechanical properties. The coating system can be expertly designed by choosing the appropriate substrate material and substrate treatment method, the type of matrix material of the coating, the type, size, content, and surface modification of the filler, and adopting appropriate coating preparation methods and parameters. In choosing a polymer, we must consider the advantages and disadvantages of the coating preparation methods. We must also understand the mechanisms for strengthening and toughening when using different fillers, and how they may improve the tribological performance of the polymer. Furthermore, using optimized methods of coating adhesion can improve the service status of the coating.

Based on our research on polymer coatings, the types and synergies of fillers are key to improving the tribological and mechanical properties of composite coatings. Previous test results indicate that layered shear and oxidation products produce excellent lubrication, as is the case with black phosphorus. Moreover, it effectively reduces the friction coefficient of polymer coatings when used as a lubricating filler. The addition of a few micro- or nano-level microcapsules also significantly reduces the friction coefficient and wear rate of the polymer coating. The above-mentioned excellent lubricating fillers combined with reinforcing phases, e.g., carbon fiber and silica nanoparticles, can maximize the load-bearing capacity of the polymer coating, and achieve a balance between good tribological performance and desirable mechanical performance. We believe that the above fillers can effectively improve the tribological properties of most polymer coatings and ensure that the mechanical properties do not cause significant attenuation.

Although research on polymer composite coatings is very extensive at present, it is still slightly insufficient compared with studies on polymer composites. For the research on polymer composite coatings, the following aspects still need to be addressed:

1) In order to achieve a balance between friction and mechanical properties of coatings, the synergistic effects of lubricating fillers and reinforcing fillers are required. Further research should be carried out to explore the synergy between different components. In recent years, some new two-dimensional materials have been researched and prepared, such as T-type carbon [213] and phosphorene [214]. New two-dimensional materials can be explored as fillers to improve the friction and mechanical properties of composite materials.

2) In the study of composite coatings covered in this review, the effect of polymer coating thickness on the performance of composite coatings remains obscure. Further studies regarding the role of thickness would be worthwhile. Most of the coatings reviewed are single-layer coatings, and designing multilayer or adaptive smart coatings should be considered.

3) The improvement of the tribological properties of the composite coating is mostly explained by the formation of a transfer film, but the specific mechanism of the formation and growth processes of the transfer film has not been proposed. Further research on the lubrication mechanism on a more microscopic scale is required. In addition, the lubrication mechanism for PS/PI blends is an anomaly, which is a structural effect rather than the formation of a transfer film. Therefore, in-depth research on the friction mechanism is needed.

4) The excellent research results of polymer block

materials should be applied to coating materials. For example, the addition of microcapsules can achieve an ultra-low friction coefficient of 0.028 for block epoxy materials. This filler formula should be applied to epoxy coatings to achieve an ultra-low friction coefficient of an epoxy coating.

5) The current trend of modern tribology is to limit or reduce the use of liquid lubricants as much as possible, but to increase the use of solid materials and coatings with self-lubricating properties. However, in the short term, the best compromise is to consider using a combination of solid and liquid lubricants to meet the emissions or environmental requirements of future tribological systems while providing the required friction and wear performance. Microcapsule technology is an effective mean to achieve this goal, but cold-pressed and hot-pressed polymer materials will cause the capsules to crack during the molding process. The spray application method of coatings may be suitable for the practical application of microcapsules. Currently, polymer coatings containing microcapsules are mostly epoxy-based. The preparation of composite coatings containing microcapsules with multiple matrices is needed.

Acknowledgements

This work was supported by National Natural Science Foundation of China (Grant No. 51822505), Beijing Natural Science Foundation of China (Grant No. 3182010), Major Scientific Research and Development Project in Jiangxi (Grant No. 20173ABC28008), and the National Key Research and Development Program of China (Grant No. 2018YFB2000202).

References

[1] Wang C, Brown G O, Burris D L, Korley L S T J, Epps III T H. Coating architects: Manipulating multiscale structures to optimize interfacial properties for coating applications. *ACS Appl Polym Mater* **1**(9): 2249–2266 (2019)

[2] Donnet C, Erdemir A. Solid lubricant coatings: Recent developments and future trends. *Tribol Lett* **17**(3): 389–397 (2004)

[3] Scharf T W, Prasad S V. Solid lubricants: A review. *J Mater Sci* **48**(2): 511–531 (2013)

[4] Sawyer W G, Freudenberg K D, Bhimaraj P, Schadler L S. A study on the friction and wear behavior of PTFE filled with alumina nanoparticles. *Wear* **254**(5–6): 573–580 (2003)

[5] Yuan H, Yang S R, Liu X H, Wang Z F, Ma L M, Hou K M, Yang Z G, Wang J Q. Polyimide-based lubricating coatings synergistically enhanced by MoS_2@HCNF hybrid. *Composites Part A* **102**: 9–17 (2017)

[6] Pan B L, Zhao J, Zhang Y Q, Zhang Y Z. Wear performance and mechanisms of polyphenylene sulfide/polytetrafluoroethylene wax composite coatings reinforced by graphene. *J Macromol Sci Part B* **51**(6): 1218–1227 (2012)

[7] Information. https://www.masterbond.com/techtips/how-optimizing-glass-transition-temperature-tg, 2020.

[8] Wan Y J, Gong L X, Tang L C, Wu L B, Jiang J X. Mechanical properties of epoxy composites filled with silane-functionalized graphene oxide. *Composites Part A* **64**: 79–89 (2014)

[9] Yang H J, Mo Q F, Li W Z, Gu F M. Preparation and properties of self-healing and self-lubricating epoxy coatings with polyurethane microcapsules containing

bifunctional linseed oil. *Polymers* **11**(10): 1578 (2019)

[10] Zhang L, Xie G X, Wu S, Peng S G, Zhang X Q, Guo D, Wen S Z, Luo J B. Ultralow friction polymer composites incorporated with monodispersed oil microcapsules. *Friction* **9**(1): 29–40 (2021)

[11] Yeh M K, Tai N H, Lin Y J. Glass transition temperature of phenolic-based nanocomposites reinforced by MWNTs and carbon fibers. *Key Eng Mater* **334**–**335**: 713–716 (2007)

[12] Information. https://polymerdatabase.com/Adhesives/Phenolic%20Adhesive.html, 2020.

[13] Information. http://www.matweb.com/search/DataSheet.aspx?MatGUID=e8a76ace259646bcb44768864d50643b&ckck=1, 2020.

[14] Ahmadijokani F, Shojaei A, Arjmand M, Alaei Y, Yan N. Effect of short carbon fiber on thermal, mechanical and tribological behavior of phenolic-based brake friction materials. *Composites Part B* **168**: 98–105 (2019)

[15] Frich D, Goranov K, Schneggenburger L, Economy J. Novel high-temperature aromatic copolyester thermosets: Synthesis, characterization, and physical properties. *Macromolecules* **29**(24): 7734–7739 (1996)

[16] Lan P X, Meyer J L, Economy J, Polycarpou A A. Unlubricated tribological performance of Aromatic Thermosetting Polyester (ATSP) coatings under different temperature conditions. *Tribol Lett* **61**(1): 10 (2016)

[17] Information. http://www.matweb.com/search/DataSheet.aspx?MatGUID=782e0115dbe44b8baeec0543c91098b0&ckck=1, 2020.

[18] Lima A M F, De Castro V G, Borges R S, Silva G G. Electrical conductivity and thermal properties of functionalized carbon nanotubes/polyurethane composites. *Polímeros* **22**(2): 117–124 (2012)

[19] Information. http://www.stug.com.au/materials/engineering-plastics-properties/min-max-operating-temperatures.php, 2020.

[20] Tayfun U, Dogan M, Bayramli E. Influence of surface modifications of flax fiber on mechanical and flow properties of thermoplastic polyurethane based eco-composites. *J Nat Fibers* **13**(3): 309–320 (2016)

[21] Zhang D Y, Ho J K L, Dong G N, Zhang H, Hua M. Tribological properties of Tin-based Babbitt bearing alloy with polyurethane coating under dry and starved lubrication conditions. *Tribol Int* **90**: 22–31 (2015)

[22] Yoonessi M, Shi Y, Scheiman D A, Lebron-Colon M, Tigelaar D M, Weiss R A, Meador M A. Graphene polyimide nanocomposites; thermal, mechanical, and high-temperature shape memory effects. *ACS Nano* **6**(9): 7644–7655 (2012)

[23] Information. https://dielectricmfg.com/knowledge-base/kapton/, 2020.

[24] Wang C Y, Lan Y F, Yu W T, Li X, Qian Y, Liu H S. Preparation of amino-functionalized graphene oxide/polyimide composite films with improved mechanical, thermal and hydrophobic properties. *Appl Surf Sci* **362**: 11–19 (2016)

[25] Wu X, Zhang Y, Du P, Jin Z Y, Zhao H C, Wang L P. Synthesis, characterization and properties of graphene-reinforced polyimide coatings. *New J Chem* **43**(15): 5697–5705 (2019)

[26] Blumm J, Lindemann A, Meyer M, Strasser C. Characterization of PTFE using advanced thermal analysis techniques. *Int J Thermophys* **31**(10): 1919–1927 (2010)

[27] Aderikha V N, Shapovalov V A, Pleskachevskii Y M. Strength characteristics, structure and wear resistance of ptfe-commercial carbon composites. *J Frict Wear* **29**(2): 120–126 (2008)

[28] Beckford S, Cai J Y, Fleming R A, Zou M. The effects of graphite filler on the tribological properties of polydopamine/PTFE coatings. *Tribol Lett* **64**(3): 42 (2016)

[29] Beckford S, Cai J Y, Chen J Y, Zou M. Use of Au nanoparticle-filled PTFE films to produce low-friction and low-wear surface coatings. *Tribol Lett* **56**(2): 223–230 (2014)

[30] Belyamani I, Hassan M K. Effect of different phosphate glass compositions on the process-induced macromolecular dynamics of polyamide 66. *Polymers* **12**(5): 1179 (2020)

[31] Information. https://omnexus.specialchem.com/selection-guide/polyamide-pa-nylon/properties-pa6-pa66, 2020.

[32] Information. http://www.matweb.com/search/DataSheet.aspx?MatGUID=e95795afec4f46539c51269e453cba2b, 2020

[33] Mu B, Wang Q H, Wang T M, Wang H G, Jian L Q. The friction and wear properties of clay filled PA66. *Polym Eng Sci* **48**(1): 203–209 (2008)

[34] Sohel M A, Mandal A, Mondal A, Pan S, SenGupta A. Thermal analysis of ABS/PA6 polymer blend using differential scanning calorimetry. *J Therm Anal Calorim* **129**(3): 1689–1695 (2017)

[35] Sun H Y, Jiang F, Lei F, Chen L, Zhang H, Leng J, Sun D Z. Graphite fluoride reinforced PA6 composites: Crystallization and mechanical properties. *Mater Today Commun* **16**: 217–225 (2018)

[36] Zhou S F, Zhang Q X, Huang J, Ding D. Friction and wear behaviors of polyamide-based composites blended with polyphenylene sulfide. *J Thermoplast Compos Mater* **27**(7):

977–991 (2014)

[37] Diaham S, Locatelli M L. Novel high glass transition polyamide-imide: T_g influence on electrical conductivity at high temperature. *IEEE Trans Dielectr Electr Insul* **22**(5): 3053–3058 (2015)

[38] Information. http://www.craftechind.com/torlon-polyamide-imide/, 2020.

[39] Information. https://www.substech.com/dokuwiki/doku.php?id=thermoplastic_polyamide-imide_pai_electrical_grade, 2020.

[40] Information. https://www.polytechindustrial.com/products/plastic-stock-shapes/torlon-4301, 2020.

[41] Saleem A, Frormann L, Iqbal A. High performance thermoplastic composites: Study on the mechanical, thermal, and electrical resistivity properties of carbon fiber-reinforced polyetheretherketone and polyethersulphone. *Polym Compos* **28**(6): 785–796 (2007)

[42] Information. https://omnexus.specialchem.com/selection-guide/polyetheretherketone-peek-thermoplastic, 2020.

[43] Pan G L, Guo Q, Tian A G, He Z Q. Mechanical behaviors of Al_2O_3 nanoparticles reinforced polyetheretherketone. *Mater Sci Eng*: *A* **492**(1–2): 383–391 (2008)

[44] Zhang G, Liao H, Li H, Mateus C, Bordes J M, Coddet C. On dry sliding friction and wear behaviour of PEEK and PEEK/SiC-composite coatings. *Wear* **260**(6): 594–600 (2006)

[45] Hou X H, Shan C X, Choy K L. Microstructures and tribological properties of PEEK-based nanocomposite coatings incorporating inorganic fullerene-like nanoparticles. *Surf Coat Technol* **202**(11): 2287–2291 (2008)

[46] You Z P, Li D G. The dynamical viscoelasticity and tensile property of new highly filled charcoal powder/ultra-high molecular weight polyethylene composites. *Mater Lett* **112**: 197–199 (2013)

[47] Suñer S, Joffe R, Tipper J L, Emami N. Ultra high molecular weight polyethylene/graphene oxide nanocomposites: Thermal, mechanical and wettability characterisation. *Composites Part B* **78**: 185–191 (2015)

[48] Pang W C, Ni Z F, Chen G M, Huang G D, Huang H D, Zhao Y W. Mechanical and thermal properties of graphene oxide/ultrahigh molecular weight polyethylene nanocomposites. *RSC Adv* **5**(77): 63063–63072 (2015)

[49] Azam M U, Samad M A. A novel organoclay reinforced UHMWPE nanocomposite coating for tribological applications. *Prog Org Coat* **118**: 97–107 (2018)

[50] Samad M A, Sinha S K. Nanocomposite UHMWPE-CNT polymer coatings for boundary lubrication on aluminium substrates. *Tribol Lett* **38**(3): 301–311 (2010)

[51] Zhang R C, Li R, Lu A, Jin Z J, Liu B Q, Xu Z B. The glass transition temperature of poly(phenylene sulfide) with various crystallinities. *Polym Int* **62**(3): 449–453 (2013)

[52] Chukov D, Nematulloev S, Zadorozhnyy M, Tcherdyntsev V, Stepashkin A, Zherebtsov D. Structure, mechanical and thermal properties of polyphenylene sulfide and polysulfone impregnated carbon fiber composites. *Polymers* **11**(4): 684 (2019)

[53] Information. https://omnexus.specialchem.com/selection-guide/polyphenylene-sulfide-pps-plastic-guide, 2020.

[54] Wu Y, Liu Q, Heng Z G, Zou H W, Chen Y, Liang M. Improved mechanical properties of graphene oxide/short carbon fiber-polyphenylene sulfide composites. *Polym Compos* **40**(10): 3866–3876 (2019)

[55] Xu H Y, Feng Z Z, Chen J M, Zhou H D. Tribological behavior of the carbon fiber reinforced polyphenylene sulfide (PPS) composite coating under dry sliding and water lubrication. *Mater Sci Eng*: *A* **416**(1–2): 66–73 (2006)

[56] Gamp K, Thomann Y, Friedrich C, Hebel A, Markgraf K, Hückstädt H, Kurz K, Mülhaupt R. Improving melt flow of polyoxymethylene ("High-Speed POM"): Additive design, melt rheology, and in situ composition gradient formation. *Macromol Mater Eng* **299**(1): 51–64 (2014)

[57] Information. http://www.goodfellow.com/E/Polyoxymethylene-Homopolymer.html, 2020.

[58] Espinach F X, Granda L A, Tarres Q, Duran J, Fullana-I-Palmer P, Mutjé P. Mechanical and micromechanical tensile strength of eucalyptus bleached fibers reinforced polyoxymethylene composites. *Composites Part B* **116**: 333–339 (2017)

[59] Huang T, Lu R G, Wang H Y, Ma Y N, Tian J S, Li T S. Investigation on the tribological properties of POM modified by nano-PTFE. *J Macromol Sci Part B* **50**(7): 1235–1248 (2011)

[60] Fakhar A, Razzaghi-Kashani M, Mehranpour M. Improvements in tribological properties of polyoxy¬methylene by aramid short fiber and polytetrafluoroe¬thylene. *Iran Polym J* **22**(1): 53–59 (2013)

[61] Wang G L, Yu D M, Kelkar A D, Zhang L F. Electrospun nanofiber: Emerging reinforcing filler in polymer matrix composite materials. *Prog Polym Sci* **75**: 73–107 (2017)

[62] Segatelli M G, Pagotto Yoshida I V, do Carmo Gonçalves M. Natural silica fiber as reinforcing filler of nylon 6. *Composites Part B* **41**(1): 98–105 (2010)

[63] Coleman J N, Khan U, Gun'ko Y K. Mechanical

reinforcement of polymers using carbon nanotubes. *Adv Mater* **18**(6): 689–706 (2006)

[64] Podsiadlo P, Kaushik A K, Arruda E M, Waas A M, Shim B S, Xu J D, Nandivada H, Pumplin B G, Lahann J, Ramamoorthy A, et al. Ultrastrong and stiff layered polymer nanocomposites. *Science* **318**(5847): 80–83 (2007)

[65] Panin S V, Duc Anh N, Kornienko L A, Ivanova L R, Ovechkin B B. Comparison on Efficiency of Solid-Lubricant Fillers for Polyetheretherketone-Based Composites. *AIP Conference Proceedings* **2051**: 020232 (2018)

[66] Cai P, Wang T M, Wang Q H. Effect of several solid lubricants on the mechanical and tribological properties of phenolic resin-based composites. *Polym Compos* **36**(12): 2203–2211 (2015)

[67] Zalaznik M, Kalin M, Novak S, Jakša G. Effect of the type, size and concentration of solid lubricants on the tribological properties of the polymer PEEK. *Wear* **364–365**: 31–39 (2016)

[68] Guo Q B, Rong M Z, Jia G L, Lau K T, Zhang M Q. Sliding wear performance of nano-SiO_2/short carbon fiber/epoxy hybrid composites. *Wear* **266**(7–8): 658–665 (2009)

[69] Meng H, Sui G X, Xie G Y, Yang R. Friction and wear behavior of carbon nanotubes reinforced polyamide 6 composites under dry sliding and water lubricated condition. *Compos Sci Technol* **69**(5): 606–611 (2009)

[70] Song H J, Zhang Z Z. Investigation of the tribological properties of polyfluo wax/polyurethane composite coating filled with nano-SiC or nano-ZrO_2. *Mater Sci Eng*: *A* **426**(1–2): 59–65 (2006)

[71] Sengupta R, Bhattacharya M, Bandyopadhyay S, Bhowmick A K. A review on the mechanical and electrical properties of graphite and modified graphite reinforced polymer composites. *Prog Polym Sci* **36**(5): 638–670 (2011)

[72] Zhai W Z, Srikanth N, Kong L B, Zhou K. Carbon nanomaterials in tribology. *Carbon* **119**: 150–171 (2017)

[73] Zhai W Z, Zhou K. Nanomaterials in superlubricity. *Adv Funct Mater* **29**(28): 1806395 (2019)

[74] Liu D, Zhao W J, Liu S, Cen Q H, Xue Q J. Comparative tribological and corrosion resistance properties of epoxy composite coatings reinforced with functionalized fullerene C60 and graphene. *Surf Coat Technol* **286**: 354–364 (2016)

[75] Lee C, Wei X D, Kysar J W, Hone J. Measurement of the elastic properties and intrinsic strength of monolayer graphene. *Science* **321**(5887): 385–388 (2008)

[76] Lee G H, Cooper R C, An S J, Lee S, Van Der Zande A, Petrone N, Hammerberg A G, Lee C, Crawford B, Oliver W, et al. High-strength chemical-vapor- deposited graphene and grain boundaries. *Science* **340**(6136): 1073–1076 (2013)

[77] Li X, Chen B B, Jia Y H, Li X F, Yang J, Li C S, Yan F Y. Enhanced tribological properties of epoxy-based lubricating coatings using carbon nanotubes-ZnS hybrid. *Surf Coat Technol* **344**: 154–162 (2018)

[78] Lee J Y, Lim D S. Tribological behavior of PTFE film with nanodiamond. *Surf Coat Technol* **188–189**: 534–538 (2004)

[79] Lee J Y, Lim D P, Lim D S. Tribological behavior of PTFE nanocomposite films reinforced with carbon nanoparticles. *Composites Part B* **38**(7–8): 810–816 (2007)

[80] Miyake S, Sekine Y, Noshiro J, Watanabe S. Low-friction and long-life solid lubricant films structured of nanoperiod tungsten disulfide and molybdenum disulfide multilayer. *Jpn J Appl Phys* **43**(7A): 4338–4343 (2004)

[81] An V, Irtegov Y, De Izarra C. Study of tribological properties of nanolamellar WS_2 and MoS_2 as additives to lubricants. *J Nanomater* **2014**: 865839 (2014)

[82] Agag T, Koga T, Takeichi T. Studies on thermal and mechanical properties of polyimide-clay nanocomposites. *Polymer* **42**(8): 3399–3408 (2001)

[83] Wang H, Zeng C C, Elkovitch M, Lee L J, Koelling K W. Processing and properties of polymeric nano-composites. *Polym Eng Sci* **41**(11): 2036–2046 (2001)

[84] Xu Q J, Feng X T, Liu J H, Gong P J. Preparation of Ag nanoparticles-reinforced polyamide 6 nanocomposites by in situ polymerization and investigation of its properties. *Pol J Chem Technol* **19**(4): 36–40 (2017)

[85] Hidayah I N, Mariatti M. Properties of single and hybrid aluminum and silver fillers filled high-density polyethylene composites. *J Thermoplast Compos Mater* **25**(2): 209–221 (2012)

[86] Li Z H, Wang D, Zhang M, Zhao L. Enhancement of the thermal conductivity of polymer composites with Ag-graphene hybrids as fillers. *Phys Status Solidi A* **211**(9): 2142–2149 (2014)

[87] Chen Y C, Zhou S X, Yang H H, Wu L M. Structure and properties of polyurethane/nanosilica composites. *J Appl Polym Sci* **95**(5): 1032–1039 (2005)

[88] Zhang G, Schlarb A K, Tria S, Elkedim O. Tensile and tribological behaviors of PEEK/nano-SiO_2 composites compounded using a ball milling technique. *Compos Sci Technol* **68**(15–16): 3073–3080 (2008)

[89] Wang Y, Gong J, Yang D Y, Gao G, Ren J F, Mu B, Chen S

S, Wang H G. Tribological behavior of nano-Al_2O_3-reinforced PPS-PTFE composites. *Tribol Trans* **57**(2): 173–181 (2014)

[90] Vaisakh S S, Mohammed A A P, Hassanzadeh M, Tortorici J F, Metz R, Ananthakumar S. Effect of nano-modified SiO_2/Al_2O_3 mixed-matrix micro-composite fillers on thermal, mechanical, and tribological properties of epoxy polymers. *Polym Adv Technol* **27**(7): 905–914 (2016)

[91] Song H H, Zhang Z Z, Men X H. The tribological behaviors of the polyurethane coating filled with nano-SiO_2 under different lubrication conditions. *Composites Part A* **39**(2): 188–194 (2008)

[92] Li H Y, Cui Y X, Wang H Y, Zhu Y J, Wang B H. Preparation and application of polysulfone microcapsules containing tung oil in self-healing and self-lubricating epoxy coating. *Colloids Surf A* **518**: 181–187 (2017)

[93] Li H Y, Cui Y X, Li Z K, Zhu Y J, Wang H Y. Fabrication of microcapsules containing dual-functional tung oil and properties suitable for self-healing and self-lubricating coatings. *Prog Org Coat* **115**: 164–171 (2018)

[94] Yang M M, Zhu X T, Ren G N, Men X H, Guo F, Li P L, Zhang Z Z. Tribological behaviors of polyurethane composite coatings filled with ionic liquid core/silica gel shell microcapsules. *Tribol Lett* **58**(1): 9 (2015)

[95] Li H Y, Li S, Li F B, Li Z K, Wang H Y. Fabrication of SiO_2 wrapped polystyrene microcapsules by Pickering polymerization for self-lubricating coatings. *J Colloid Interface Sci* **528**: 92–99 (2018)

[96] Pathania A, Arya R K, Ahuja S. Crosslinked polymeric coatings: Preparation, characterization, and diffusion studies. *Prog Org Coat* **105**: 149–162 (2017)

[97] Wu X, Wyman I, Zhang G W, Lin J, Liu Z Q, Wang Y, Hu H. Preparation of superamphiphobic polymer-based coatings via spray- and dip-coating strategies. *Prog Org Coat* **90**: 463–471 (2016)

[98] Moridi A, Hassani-Gangaraj S M, Guagliano M, Dao M. Cold spray coating: Review of material systems and future perspectives. *Surf Eng* **30**(6): 369–395 (2014)

[99] Petrovicova E, Schadler L S. Thermal spraying of polymers. *Int Mater Rev* **47**(4): 169–190 (2002)

[100] Na J Y, Kang B, Sin D H, Cho K, Park Y D. Understanding solidification of polythiophene thin films during spin-coating: Effects of spin-coating time and processing additives. *Sci Rep* **5**(1): 13288 (2015)

[101] Hou L T, Wang E G, Bergqvist J, Andersson B V, Wang Z Q, Müller C, Campoy-Quiles M, Andersson M R, Zhang F L, Inganäs O. Lateral phase separation gradients in spin-coated thin films of high-performance polymer: Fullerene photovoltaic blends. *Adv Funct Mater* **21**(16): 3169–3175 (2011)

[102] Campbell S E, Collins M, Xie L, Belbruno J J. Surface morphology of spin-coated molecularly imprinted polymer films. *Surf Interface Anal* **41**(4): 347–356 (2009)

[103] Singh-Beemat J, Iroh J O. The effect of morphology on the corrosion inhibition and mechanical properties of hybrid polymer coatings. *J Appl Polym Sci* **128**(3): 1616–1624 (2013)

[104] Dário A F, Macia H B, Petri D F S. Nanostructures on spin-coated polymer films controlled by solvent composition and polymer molecular weight. *Thin Solid Films* **524**: 185–190 (2012)

[105] Li X, Han Y C, An L J. Surface morphology control of immiscible polymer-blend thin films. *Polymer* **44**(26): 8155–8165 (2003)

[106] Li Y, Hu K, Han X, Yang Q Y, Xiong Y F, Bai Y H, Guo X, Cui Y S, Yuan C S, Ge H X, et al. Phase separation of silicon-containing polymer/polystyrene blends in spin-coated films. *Langmuir* **32**(15): 3670–3678 (2016)

[107] Cui L, Li X, Han Y C. Polymer concentration, shear and stretch field effects on the surface morphology evolution during the spin-coating. *Appl Surf Sci* **252**(23): 8156–8162 (2006)

[108] Petri D F S. Characterization of spin-coated polymer films. *J Braz Chem Soc* **13**(5): 695–699 (2002)

[109] Roy S, Ansari K J, Jampa S S K, Vutukuri P, Mukherjee R. Influence of substrate wettability on the morphology of thin polymer films spin-coated on topographically patterned substrates. *ACS Appl Mater Interfaces* **4**(4): 1887–1896 (2012)

[110] Vital A, Vayer M, Tillocher T, Dussart R, Boufnichel M, Sinturel C. Morphology control in thin films of PS: PLA homopolymer blends by dip-coating deposition. *Appl Surf Sci* **393**: 127–133 (2017)

[111] Jiang J H, Zhu L P, Zhu L J, Zhu B K, Xu Y Y. Surface characteristics of a self-polymerized dopamine coating deposited on hydrophobic polymer films. *Langmuir* **27**(23): 14180–14187 (2011)

[112] Van Stam J, Van Fraeyenhoven P, Andersen M, Moons E. Comparing morphology in dip-coated and spin-coated polyfluorene: Fullerene films. *Proceedings of SPIE* **9942**: 99420D (2016)

[113] Van Stam J, Van Fraeyenhoven P, Andersen M, Moons E. Comparing morphology in dip-coated and spin-coated polyfluorene: Fullerene films. In *Proceedings of SPIE 9942*,

Organic Photovoltaics XVII, San Diego, 2016: 99420D.

[114] Leivo E, Wilenius T, Kinos T, Vuoristo P, Mäntylä T. Properties of thermally sprayed fluoropolymer PVDF, ECTFE, PFA and FEP coatings. *Prog Org Coat* **49**(1): 69–73 (2004)

[115] Han J, Ding S Y, Zheng W G, Li W Y, Li H. Microstructure and anti- wear and corrosion performances of novel UHMWPE/graphene-nanosheet composite coatings deposited by flame spraying. *Polym Adv Technol* **24**(10): 888–894 (2013)

[116] Bao Y, Gawne D T, Vesely D, Bevis M J. Production of polymer matrix composite coatings by thermal spraying. *Trans IMF* **72**(3): 110–113 (1994)

[117] Petrovicova E, Knight R, Schadler L S, Twardowski T E. Nylon 11/silica nanocomposite coatings applied by the HVOF process. I. Microstructure and morphology. *J Appl Polym Sci* **77**(8): 1684–1699 (2000)

[118] Khalkhali Z, Rothstein J P. Characterization of the cold spray deposition of a wide variety of polymeric powders. *Surf Coat Technol* **383**: 125251 (2020)

[119] Baum M J, Heepe L, Gorb S N. Friction behavior of a microstructured polymer surface inspired by snake skin. *Beilstein J Nanotechnol* **5**: 83–97 (2014)

[120] Song J F, Liu X L, Zhao G, Ding Q J, Qiu J H. Effect of surface roughness and reciprocating time on the tribological properties of the polyimide composites. *Polym Eng Sci* **59**(3): 483–489 (2019)

[121] Zhang G, Liao H L, Coddet C. Friction and wear behavior of PEEK and its composite coatings. *Tribol Interface Eng Ser* **55**: 458–482. (2008)

[122] Zhang G, Häusler I, Österle W, Wetzel B, Jim B. Formation and function mechanisms of nanostructured tribofilms of epoxy-based hybrid nanocomposites. *Wear* **342**–343: 181–188 (2015)

[123] Fan X F, Li G T, Guo Y X, Zhang L G, Xu Y K, Zhao F Y, Zhang G. Role of reinforcement types and silica nanoparticles on tribofilm growth at PTFE-Steel interface. *Tribol Int* **143**: 106035 (2020)

[124] Hu C, Qi H M, Yu J X, Zhang G, Zhang Y F, He H T. Significant improvement on tribological performance of polyimide composites by tuning the tribofilm nanostructures. *J Mater Process Technol* **281**: 116602 (2020)

[125] Zhang G, Österle W, Jim B, Häusler I, Hesse R, Wetzel B. The role of surface topography in the evolving microstructure and functionality of tribofilms of an epoxy-based nanocomposite. *Wear* **364**–**365**: 48–56 (2016)

[126] Guo L H, Zhang G, Wang D A, Zhao F Y, Wang T M, Wang Q H. Significance of combined functional nanoparticles for enhancing tribological performance of PEEK reinforced with carbon fibers. *Composites Part A* **102**: 400–413 (2017)

[127] Biswas S K, Vijayan K. Friction and wear of ptfe – A review. *Wear* **158**(1–2): 193–211 (1992)

[128] Nemati N, Emamy M, Yau S, Kim J K, Kim D E. High temperature friction and wear properties of graphene oxide/polytetrafluoroethylene composite coatings deposited on stainless steel. *RSC Adv* **6**(7): 5977–5987 (2016)

[129] Ding Q J, Zhang Y D, Zhao G, Wang F. Properties of POB reinforced PTFE-based friction material for ultrasonic motors. *J Polym Eng* **37**(7): 681–687 (2017)

[130] Lim W S, Khadem M, Anle Y, Kim D E. Fabrication of polytetrafluoroethylene-carbon nanotube composite coatings for friction and wear reduction. *Polym Compos* **39**(S2): E710–E722 (2018)

[131] McCook N L, Burris D L, Bourne G R, Steffens J, Hanrahan J R, Sawyer W G. Wear resistant solid lubricant coating made from PTFE and epoxy. *Tribol Lett* **18**(1): 119–124 (2005)

[132] Peng S G, Zhang L, Xie G X, Guo Y, Si L N, Luo J B. Friction and wear behavior of PTFE coatings modified with poly (methyl methacrylate). *Composites Part B* **172**: 316–322 (2019)

[133] Su F H, Zhang S H. Tribological properties of polyimide coatings filled with PTFE and surface-modified nano-Si_3N_4. *J Appl Polym Sci* **131**(12): 40410 (2014)

[134] Luo Z Z, Zhang Z Z, Wang W J, Liu W M. Effect of polytetrafluoroethylene gradient-distribution on the hydrophobic and tribological properties of polyphenylene sulfide composite coating. *Surf Coat Technol* **203**(10–11): 1516–1522 (2009)

[135] [134] Yu C Y, Wan H Q, Chen L, Li H X, Cui H X, Ju P F, Zhou H D, Chen J M. Marvelous abilities for polyhedral oligomeric silsesquioxane to improve tribological properties of polyamide-imide/polytetrafluoroethylene coatings. *J Mater Sci* **53**(17): 12616–12627 (2018)

[136] Akram M W, Meyer J L, Polycarpou A A. Tribological interactions of advanced polymeric coatings with polyalkylene glycol lubricant and r1234yf refrigerant. *Tribol Int* **97**: 200–211 (2016)

[137] Bashandeh K, Lan P X, Meyer J L, Polycarpou A A. Tribological performance of graphene and PTFE solid lubricants for polymer coatings at elevated temperatures. *Tribol Lett* **67**(3): 99 (2019)

[138] Yu C Y, Ju P F, Wan H Q, Chen L, Li H X, Zhou H D, Chen

J M. POSS-Grafted PAI/MoS_2 coatings for simultaneously improved tribological properties and atomic oxygen resistance. *Ind Eng Chem Res* **58**(36): 17027–17037 (2019)

[139] Xu H Y, Feng Z Z, Chen J M, Zhou H D. Tribological behavior of the polyamide composite coating filled with different fillers under dry sliding. *J Appl Polym Sci* **104**(4): 2554–2560 (2007)

[140] Wang W, Xie G X, Luo J B. Black phosphorus as a new lubricant. *Friction* **6**(1): 116–142 (2018)

[141] Lv Y, Wang W, Xie G X, Luo J B. Self-lubricating PTFE-based composites with black phosphorus nanosheets. *Tribol Lett* **66**(2): 61 (2018)

[142] Wang W, Xie G X, Luo J B. Superlubricity of black phosphorus as lubricant additive. *ACS Appl Mater Interfaces* **10**(49): 43203–43210 (2018)

[143] Bai L C, Liu B, Srikanth N, Tian Y, Zhou K. Nano-friction behavior of phosphorene. *Nanotechnology* **28**(35): 355704 (2017)

[144] Ren X Y, Yang X, Xie G X, Luo J B. Black phosphorus quantum dots in aqueous ethylene glycol for macroscale superlubricity. *ACS Appl Nano Mater* **3**(5): 4799–4809 (2020)

[145] Peng S G, Guo Y, Xie G X, Luo J B. Tribological behavior of polytetrafluoroethylene coating reinforced with black phosphorus nanoparticles. *Appl Surf Sci* **441**: 670–677 (2018)

[146] Wu S, He F, Xie G X, Bian Z L, Luo J B, Wen S Z. Black phosphorus: Degradation favors lubrication. *Nano Lett* **18**(9): 5618–5627 (2018)

[147] Wu S, He F, Xie G X, Bian Z L, Ren Y L, Liu X Y, Yang H J, Guo D, Zhang L, Wen S Z, et al. Super-slippery degraded black phosphorus/silicon dioxide interface. *ACS Appl Mater Interfaces* **12**(6): 7717–7726 (2020)

[148] Kurdi A, Li C. Comparative tribological and mechanical property analysis of nano-silica and nano-rubber reinforced epoxy composites. *Appl Mech Mater* **875**: 53–60 (2018)

[149] Zhang G L, Xie G X, Si L N, Wen S Z, Guo D. Ultralow friction self-lubricating nanocomposites with mesoporous metal–organic frameworks as smart nanocontainers for lubricants. *ACS Appl Mater Interfaces* **9**(43): 38146–38152 (2017)

[150] Li H Y, Wang Q, Wang H Y, Cui Y X, Zhu Y J, Wang B H. Fabrication of thermally stable polysulfone microcapsules containing [EMIm] [NTf_2] ionic liquid for enhancement of in situ self-lubrication effect of epoxy. *Macromol Mater Eng* **301**(12): 1473–1481 (2016)

[151] Li H Y, Li S, Li Z K, Zhu Y J, Wang H Y. Polysulfone/SiO_2 hybrid shell microcapsules synthesized by the combination of pickering emulsification and the solvent evaporation technique and their application in self-lubricating composites. *Langmuir* **33**(49): 14149–14155 (2017)

[152] Li K K, Li H Y, Cui Y X, Li Z K, Ji J, Feng Y Y, Chen S J, Zhang M J, Wang H Y. Dual-functional coatings with self-lubricating and self-healing properties by combining Poly(urea-formaldehyde)/SiO_2 hybrid microcapsules containing linseed oil. *Ind Eng Chem Res* **58**(48): 22032–22039 (2019)

[153] Kurdi A, Chang L. Recent advances in high performance polymers-tribological aspects. *Lubricants* **7**(1): 2 (2019)

[154] Qi H M, Zhang G, Chang L, Zhao F Y, Wang T M, Wang Q H. Ultralow friction and wear of polymer composites under extreme unlubricated sliding conditions. *Adv Mater Interfaces* **4**(13): 1601171 (2017)

[155] Zhang Y C, Zhang D Y, Wei X, Zhong S J, Wang J L. Enhanced tribological properties of polymer composite coating containing graphene at room and elevated temperatures. *Coatings* **8**(3): 91 (2018)

[156] Song H J, Zhang Z Z, Men X H. Tribological behavior of polyurethane-based composite coating reinforced with TiO_2 nanotubes. *Eur Polym J* **44**(4): 1012–1022 (2008)

[157] Song H J, Zhang Z Z, Men X H. Surface-modified carbon nanotubes and the effect of their addition on the tribological behavior of a polyurethane coating. *Eur Polym J* **43**(10): 4092–4102 (2007)

[158] Pan G L, Guo Q, Ding J, Zhang W D, Wang X M. Tribological behaviors of graphite/epoxy two-phase composite coatings. *Tribol Int* **43**(8): 1318–1325 (2010)

[159] Wang C J, Wang H Y, Li M L, Liu Z J, Lv C J, Zhu Y J, Bao N Z. Anti-corrosion and wear resistance properties of polymer composite coatings: Effect of oily functional fillers. *J Taiwan Inst Chem Eng* **85**: 248–256 (2018)

[160] Song H H, Zhang Z Z, Luo Z Z. Effects of solid lubricants on friction and wear behaviors of the phenolic coating under different friction conditions. *Surf Coat Technol* **201**(6): 2760–2767 (2006)

[161] Yang M M, Zhang Z Z, Zhu X T, Men X H, Ren G N. *In situ* reduction and functionalization of graphene oxide to improve the tribological behavior of a phenol formaldehyde composite coating. *Friction* **3**(1): 72–81 (2015)

[162] Wang J, Zhao W Z, Guo C W. Fabrication and properties of a lubrication composite coating based on poly (*p*-hydroxybenzoic acid) (PHBA). *J Mater Sci* **44**(1): 227–233 (2009)

[163] Ye X Y, Liu X H, Yang Z G, Wang Z F, Wang H G, Wang J

Q, Yang S R. Tribological properties of fluorinated graphene reinforced polyimide composite coatings under different lubricated conditions. *Composites Part A* **81**: 282–288 (2016)

[164] Pozdnyakov A O, Kudryavtsev V V, Friedrich K. Sliding wear of polyimide-C_{60} composite coatings. Wear **254**(5–6): 501–513 (2003)

[165] Pei X Q, Bennewitz R, Kasper C, Tlatlik H, Bentz D, Becker-Willinger C. Tribological synergy of filler components in multifunctional polyimide coatings. *Adv Eng Mater* **19**(1): 1600363 (2017)

[166] Hedayati M, Salehi M, Bagheri R, Panjepour M, Naeimi F. Tribological and mechanical properties of amorphous and semi-crystalline PEEK/SiO_2 nanocomposite coatings deposited on the plain carbon steel by electrostatic powder spray technique. *Prog Org Coat* **74**(1): 50–58 (2012)

[167] Samad M A, Sinha S K. Mechanical, thermal and tribological characterization of a UHMWPE film reinforced with carbon nanotubes coated on steel. *Tribol Int* **44**(12): 1932–1941 (2011)

[168] Aliyu I K, Mohammed A S, Al-Qutub A. Tribological performance of UHMWPE/GNPs nanocomposite coatings for solid lubrication in bearing applications. *Tribol Lett* **66**(4): 144 (2018)

[169] Beckford S, Mathurin L, Chen J Y, Fleming R A, Zou M. The effects of polydopamine coated Cu nanoparticles on the tribological properties of polydopamine/PTFE coatings. *Tribol Int* **103**: 87–94 (2016)

[170] Pryamitsyn V, Ganesan V. Origins of linear viscoelastic behavior of polymer-nanoparticle composites. *Macromolecules* **39**(2): 844–856 (2006)

[171] Mujtaba A, Keller M, Ilisch S, Radusch H J, Beiner M, Thurn-Albrecht T, Saalwächter K. Detection of surface-immobilized components and their role in viscoelastic reinforcement of rubber-silica nanocomposites. *ACS Macro Lett* **3**(5): 481–485 (2014)

[172] Chen Q, Gong S S, Moll J, Zhao D, Kumar S K, Colby R H. Mechanical reinforcement of polymer nanocomposites from percolation of a nanoparticle network. *ACS Macro Lett* **4**(4): 398–402 (2015)

[173] Papon A, Montes H, Lequeux F, Oberdisse J, Saalwächter K, Guy L. Solid particles in an elastomer matrix: Impact of colloid dispersion and polymer mobility modification on the mechanical properties. *Soft Matter* **8**(15): 4090–4096 (2012)

[174] Papageorgiou D G, Li Z L, Liu M F, Kinloch I A, Young R J. Mechanisms of mechanical reinforcement by graphene and carbon nanotubes in polymer nanocomposites. *Nanoscale* **12**(4): 2228–2267 (2020)

[175] Chih A, Ansón-Casaos A, Puértolas J A. Frictional and mechanical behaviour of graphene/UHMWPE composite coatings. *Tribol Int* **116**: 295–302 (2017)

[176] Fu S Y, Feng X Q, Lauke B, Mai Y W. Effects of particle size, particle/matrix interface adhesion and particle loading on mechanical properties of particulate-polymer composites. *Composites Part B* **39**(6): 933–961 (2008)

[177] Reynaud E, Jouen T, Gauthier C, Vigier G, Varlet J. Nanofillers in polymeric matrix: A study on silica reinforced PA6. *Polymer* **42**(21): 8759–8768 (2001)

[178] Maillard D, Kumar S K, Fragneaud B, Kysar J W, Rungta A, Benicewicz B C, Deng H, Brinson L C, Douglas J F. Mechanical properties of thin glassy polymer films filled with spherical polymer-grafted nanoparticles. *Nano Lett* **12**(8): 3909–3914 (2012)

[179] Mortazavian S, Fatemi A. Effects of fiber orientation and anisotropy on tensile strength and elastic modulus of short fiber reinforced polymer composites. *Composites Part B* **72**: 116–129 (2015)

[180] Bonderer L J, Studart A R, Gauckler L J. Bioinspired design and assembly of platelet reinforced polymer films. *Science* **319**(5866): 1069–1073 (2008)

[181] Chan M L, Lau K T, Wong T T, Ho M P, Hui D. Mechanism of reinforcement in a nanoclay/polymer composite. *Composites Part B* **42**(6): 1708–1712 (2011)

[182] Shelley J S, Mather P T, DeVries K L. Reinforcement and environmental degradation of nylon-6/clay nanocomposites. *Polymer* **42**(13): 5849–5858 (2001)

[183] Cheng S W, Bocharova V, Belianinov A, Xiong S M, Kisliuk A, Somnath S, Holt A P, Ovchinnikova O S, Jesse S, Martin H, et al. Unraveling the mechanism of nanoscale mechanical reinforcement in glassy polymer nanocomposites. *Nano Lett* **16**(6): 3630–3637 (2016)

[184] Okumura T, Sonobe K, Ohashi A, Watanabe H, Watanabe K, Oyamada H, Aramaki M, Ougizawa T. Synthesis of polyamide‐hydroxyapatite nanocomposites. *Polym Eng Sci* **60**(7): 1699–1711 (2020)

[185] Scotti R, Conzatti L, D'Arienzo M, Di Credico B, Giannini L, Hanel T, Stagnaro P, Susanna A, Tadiello L, Morazzoni F. Shape controlled spherical (0D) and rod-like (1D) silica nanoparticles in silica/styrene butadiene rubber nanocomposites: Role of the particle morphology on the filler reinforcing effect. *Polymer* **55**(6): 1497–1506 (2014)

[186] Pradhan S, Lach R, Le H H, Grellmann W, Radusch H J, Adhikari R. Effect of filler dimensionality on mechanical

properties of nanofiller reinforced polyolefin elastomers. *Int Sch Res Not* **2013**: 284504 (2013)

[187] Nadiv R, Shachar G, Peretz-Damari S, Varenik M, Levy I, Buzaglo M, Ruse E, Regev O. Performance of nano-carbon loaded polymer composites: Dimensionality matters. *Carbon* **126**: 410–418 (2018)

[188] Bhandari N L, Lach R, Grellmann W, Adhikari R. Depth-dependent indentation microhardness studies of different polymer nanocomposites. *Macromol Symp* **315**(1): 44–51 (2012)

[189] Opelt C V, Becker D, Lepienski C M, Coelho L A F. Reinforcement and toughening mechanisms in polymer nanocomposites - Carbon nanotubes and aluminum oxide. *Composites Part B* **75**: 119–126 (2015)

[190] Wei Y Z, Wang G S, Wu Y, Yue Y H, Wu J T, Lu C, Guo L. Bioinspired design and assembly of platelet reinforced polymer films with enhanced absorption properties. *J Mater Chem A* **2**(15): 5516–5524 (2014)

[191] He Y, Farokhzadeh K, Edrisy A. Characterization of thermal, mechanical and tribological properties of fluoropolymer composite coatings. *J Mater Eng Perform* **26**(6): 2520–2534 (2017)

[192] Su C, Xue F, Li T S, Xin Y S, Wang M M. Study on the tribological properties of carbon fabric/polyimide composites filled with SiC nanoparticles. *J Macromol Sci Part B* **55**(6): 627–641 (2016)

[193] Huang T, Li T S, Xin Y S, Liu P, Su C. Mechanical and tribological properties of hybrid fabric-modified polyetherimide composites. *Wear* **306**(1–2): 64–72 (2013)

[194] Browning R L, Lim G T, Moyse A, Sue H J, Chen H, Earls J D. Quantitative evaluation of scratch resistance of polymeric coatings based on a standardized progressive load scratch test. *Surf Coat Technol* **201**(6): 2970–2976 (2006)

[195] Chen X M, Shaw C, Gelman L, Grattan K T V. Advances in test and measurement of the interface adhesion and bond strengths in coating-substrate systems, emphasising blister and bulk techniques. *Measurement* **139**: 387–402 (2019)

[196] Hopkins C, McHugh P E, O'Dowd N P, Rochev Y, McGarry J P. A combined computational and experimental methodology to determine the adhesion properties of stent polymer coatings. *Comput Mater Sci* **80**: 104–112 (2013)

[197] Czarnecki L, Garbacz A, Krystosiak M. On the ultrasonic assessment of adhesion between polymer coating and concrete substrate. *Cem Concr Compos* **28**(4): 360–369 (2006)

[198] Van Tijum R, Vellinga W P, De Hosson J T M. Adhesion along metal-polymer interfaces during plastic deformation. *J Mater Sci* **42**(10): 3529–3536 (2007)

[199] Van Den Brand J, Van Gils S, Beentjes P C J, Terryn H, Sivel V, De Wit J H W. Improving the adhesion between epoxy coatings and aluminium substrates. *Prog Org Coat* **51**(4): 339–350 (2004)

[200] Van Dam J P B, Abrahami S T, Yilmaz A, Gonzalez-Garcia Y, Terryn H, Mol J M C. Effect of surface roughness and chemistry on the adhesion and durability of a steel-epoxy adhesive interface. *Int J Adhes Adhes* **96**: 102450 (2020)

[201] Krzywiński K, Sadowski L. The effect of texturing of the surface of concrete substrate on the pull-off strength of epoxy resin coating. *Coatings* **9**(2): 143 (2019)

[202] Jaeho K, Choi J H, Sung M, Yu W R. Improved adhesion of metal-polymer sandwich composites using a spontaneous polymer grafting process. *Funct Compos Struct* **1**(2): 025004 (2019)

[203] Choi J, Cho S B, Lee B S, Joung Y K, Park K, Han D K. Improvement of interfacial adhesion of biodegradable *polymers* coated on metal surface by nanocoupling. *Langmuir* **27**(23): 14232–14239 (2011)

[204] Bedair T M, Cho Y, Kim T J, Kim Y D, Park B J, Joung Y K, Han D K. Reinforcement of interfacial adhesion of a coated polymer layer on a cobalt-chromium surface for drug-eluting stents. *Langmuir* **30**(27): 8020–8028 (2014)

[205] Chen H, Wang J H, Huo Q. Self-assembled monolayer of 3-aminopropyltrimethoxysilane for improved adhesion between aluminum alloy substrate and polyurethane coating. *Thin Solid Films* **515**(18): 7181–7189 (2007)

[206] Brostow W, Chen I K, Hnatchuk N, Hrbacek J, Hull A, Pahler R H, Srinivasan A. Enhanced adhesion of polypropylene to copper substrates. *Polym Test* **63**: 158–162 (2017)

[207] Dong F, Meschter S J, Cho J. Improved adhesion of polyurethane-based coatings to tin surface. *J Mater Sci*: *Mater Electron* **30**(8): 7268–7279 (2019)

[208] Rohart V, Laberge Lebel L, Dubé M. Improved adhesion between stainless steel heating element and PPS polymer in resistance welding of thermoplastic composites. *Composites Part B* **188**: 107876 (2020)

[209] Seul S D, Lim J M, Ha S H, Kim Y H. Adhesion enhancement of polyurethane coated leather and polyurethane foam with plasma treatment. *Korean J Chem Eng* **22**(5): 745–749 (2005)

[210] Mui T S M, Silva L L G, Prysiazhnyi V, Kostov K G. Polyurethane paint adhesion improvement on aluminium alloy treated by plasma jet and dielectric barrier discharge.

J Adhes Sci Technol **30**(2): 218–229 (2016)

[211] Ohkubo Y, Ishihara K, Sato H, Shibahara M, Nagatani A, Honda K, Endo K, Yamamura Y. Adhesive-free adhesion between polytetrafluoroethylene (PTFE) and isobutylene-isoprene rubber (IIR) via heat-assisted plasma treatment. *RSC Adv* **7**(11): 6432–6438 (2017)

[212] Ohkubo Y, Nakagawa T, Endo K, Yamamura K. Influence of air contamination during heat-assisted plasma treatment on adhesion properties of polytetrafluoroethylene (PTFE). *RSC Adv* **9**(40): 22900–22906 (2019)

[213] Hamdi M, Saleh M N, Poulis J A. Improving the adhesion strength of polymers: Effect of surface treatments. *J Adhes Sci Technol* 34(17): 1853–1870 (2020)

[214] Bai L C, Sun P P, Liu B, Liu Z S, Zhou K. Mechanical behaviors of T-carbon: A molecular dynamics study. *Carbon* 138: 357–362 (2018)

[215] Liu B, Bai L C, Korznikova E A, Dmitriev S V, Law A W K, Zhou K. Thermal conductivity and tensile response of phosphorene nanosheets with vacancy defects. *J Phys Chem C* **121**(25): 13876–13887 (2017)

Yilong REN. He received his B.S. degree in materials science and engineering from University of Science and Technology Beijing in 2018, and he is currently perusing a Ph.D. from Tsinghua University. His research interests are mainly about solid lubricating materials and wear monitoring technology.

Guoxin XIE. He received his Ph.D. degree at Tsinghua University, China, in 2010, majoring in mechanical engineering. After that, he spent two years at State Key Laboratory of Tribology, Tsinghua University, China for postdoctoral research. From 2012 to 2014, he worked at Royal Institute of Technology, Sweden, for another two-year post-doctoral research. Since 2014, he has worked at Tsinghua University as an associate professor. His research interests include intelligent self-lubrication, electric contact lubrication, etc. He has published more than 50 referred papers in international journals. He won several important academic awards, such as Chinese Thousands of Young Talents, the Excellent Doctoral Dissertation Award of China, and Ragnar Holm Plaque from KTH, Sweden.

Jianbin LUO. He received his BEng degree from Northeastern University in 1982, and got his MEng degree from Xi'an University of Architecture and Technology in 1988. In 1994, he received his Ph.D. degree from Tsinghua University and then joined the faculty of Tsinghua University. Prof. Jianbin Luo is an academician of the Chinese Academy of Sciences and a Yangtze River Scholar Distinguished Professor of Tsinghua University, Beijing, China. He was awarded the STLE International Award (2013), the Chinese National Technology Progress Prize (2008), the Chinese National Natural Science Prize (2001), and the Chinese National Invention Prize (1996). Prof. Luo has been engaged in the research of thin film lubrication and tribology in nanomanufacturing. He has been invited as a keynote or plenary speaker for 20 times on the international conferences.